

A random walk with heavy flavours

Surasree Mazumder^{†1}, Trambak Bhattacharyya^{†2} and Santosh K. Das^{*3}

[†] Variable Energy Cyclotron Center, 1/AF, Bidhan Nagar, Kolkata-700064, India

^{*} Department of Physics and Astronomy, University of Catania, Via S. Sofia 64, I-95125 Catania, Italy

Abstract

We focus on evaluating transport coefficients like drag and diffusion of heavy quarks (HQ) passing through Quark Gluon Plasma using perturbative QCD (pQCD). Experimental observable like nuclear suppression factor (R_{AA}) of HQ is evaluated for both zero and non-zero baryonic chemical potential (μ_B) scenarios using Fokker-Planck equation. Theoretical estimates of R_{AA} are contrasted with experiments.

1 Introduction:

When nuclear matter is subjected to an ambience of very high density, the individual quarks and gluons would no longer be confined within the hadrons but melt into a deconfined state of quarks and gluons. Just after the discovery of asymptotic freedom [1, 2, 3], Collins and Perry [4] also suggested that at very high density the degrees of freedom of the strongly interacting matters are not hadrons but quarks and gluons. The same is true when QCD vacuum is excited to high temperatures, too ([5]). With increasing temperature, new and new hadrons are produced thereby increasing the corresponding number density; and at a certain temperature, there is an overlap of hadrons. Such a phase of matter is called Quark Gluon Plasma (QGP) and its study needs QCD, the theory of strong interaction which is extremely successful in vacuum, to be applied in a thermal medium. So, the deconfined state of quarks and gluons gives an opportunity to peruse ‘condensed matter physics’ of elementary particles in the new domain of non-abelian gauge theory.

Lattice QCD based calculations predict that the typical value of the temperature for the quark-hadron transition, T_c , is ~ 170 MeV [6]⁴. According to the cosmological big

¹surasree.mazumder@gmail.com

²trambak.bhattacharyya@gmail.com

³dsantoshphy@gmail.com

⁴Latest lattice QCD results show that $T_c \sim 160$ MeV [7, 8, 9]

bang model the universe has undergone several phase transitions (GUT, Electroweak, quark to hadron etc) at different stages of its evolution. The quark-hadron transition occurred when the universe was few microseconds (μs) old and this is the only transition which can be accessed in the laboratory currently. The study of quark-hadron transition demands special importance in understanding the evolution of the μs old early universe. The issue is very crucial for astrophysics too, as the core of the compact astrophysical objects like neutron stars may contain quark matter at high baryon density and low temperature. So there is a multitude of reasons behind creating QGP in laboratories.

Temperature and energy density required to produce QGP in the laboratory can be achieved by colliding heavy ions at relativistic energies, under controlled laboratory environment. The nuclear collisions at Relativistic Heavy Ion Collider (RHIC) and the Large Hadron Collider (LHC) energies (200 GeV/A and 2.76 TeV/A respectively) are aimed at creating QGP. Once the QGP medium is created, we must try to understand the transport properties of the medium *i.e.* whether it is liquid or gas. The study of the transport coefficients of strongly correlated system is a field of high contemporary interest both theoretically and experimentally. In one hand, the calculation of the lower bound on the shear viscosity (η) to entropy density (s) ratio (η/s) within the frame work of AdS/CFT model [10] has ignited enormous interests among the theorists. On the other hand, the experimental study of the η/s for cold atomic systems and QGP and their similarities have generated huge interest across various branches of physics (see [11] for a review).

In general, the interaction of probes with a medium brings out useful information about the nature of the medium. As the magnitude of the transport coefficients are sensitive to the coupling strength, so these quantities qualify as useful quantities to characterize a medium.

In context of probing QGP, the heavy quarks (HQs), mainly, charm and bottom quarks, play a vital role. The reasons are as follows:

- HQ mass is significantly larger than the typically attained temperatures and other nonperturbative scales, $M \gg T_c, \Lambda_{QCD}$ (intrinsic energy scale for the strong interaction), *i.e.* the production of HQs is essentially constrained to the early, primordial stage of a heavy-ion collision and they do not dictate the bulk properties of the matter. Therefore, the heavy flavours are the witness to the entire space-time evolution of the system.
- Their thermalization time scale is larger by a factor of m/T , where m is the mass of heavy quarks and T is the temperature, than that of the light quarks and gluons and hence heavy quarks can retain the interaction history very effectively.

From experimental point of view, however, the issue of HQ thermalization in QGP can be addressed by measuring the elliptic flow (v_2) of leptons from the decays of HQs. Moreover, the observed transverse momentum suppression (R_{AA}) of leptons originating from the decays of D and B mesons produced in nuclear collisions as compared to those produced in proton+proton (pp) collisions at the same colliding energy [12, 13, 14] offer us

an opportunity to estimate the drag and diffusion coefficients of QGP⁵. Hence, no wonder that in the recent past large number of attempts have been made to study both heavy flavour suppression [12, 13] and elliptic flow [15] within the framework of perturbative QCD (pQCD) [17, 18, 19, 20, 21, 22, 23, 24, 25, 26, 27, 28, 29, 30, 31, 32, 33].

2 Motion of Heavy Quarks (HQs) in QGP:

In the introduction we have already discussed that HQs act as effective probes to look into the properties of QGP. As HQs are much heavier than the particles constituting the QGP thermal bath, one expects that they will execute brownian motion in QGP medium [34, 35]. The system under study, then, would have two components: (i) the QGP formed at an initial temperature T_i and initial thermalization time τ_i consisting of light quarks and gluons and (ii) Heavy Quark, the Brownian particle formed due to hard collisions at very early stage of heavy ion collision. The momentum distribution of HQ is governed by a non-linear integro differential equation which is the Boltzman Transport Equation (BTE):

$$\left[\frac{\partial}{\partial t} + \frac{\mathbf{p}}{E} \cdot \frac{\partial}{\partial \mathbf{x}} + \mathbf{F} \cdot \frac{\partial}{\partial \mathbf{p}} \right] f(\mathbf{x}, \mathbf{p}, t) = \left[\frac{\partial f}{\partial t} \right]_{\text{collisions}} \quad (1)$$

\mathbf{F} is the force exerted on the HQ by the surrounding colour field. \mathbf{p} and E denote the three momentum and the energy of the HQ respectively. The right hand side of Eq. 1, which is called the collision integral, $C[f]$, is attributed to the QCD interactions of HQ with light quarks (q), anti-quarks (\bar{q}) and gluons (g). One should, in principle, solve this differential equation under the influence of potential involving interaction of HQs with light quarks/anti-quarks and the background colour field in the force term. But, here, we will set $\mathbf{F} = 0$ and will treat QGP to be uniform. Therefore, the second and the third term of the left hand side of Eq. 1 vanish under these approximations. Again defining,

$$f(\mathbf{p}, t) = \frac{1}{V} \int d^3\mathbf{x} f(\mathbf{x}, \mathbf{p}, t) \quad (2)$$

which is the normalized probability distribution in the momentum space, we have

$$\frac{\partial f(\mathbf{p}, t)}{\partial t} = \left[\frac{\partial f}{\partial t} \right]_{\text{collisions}}. \quad (3)$$

Eq. 3 signifies that all variation of the distribution function of HQ with time is due to the collisions only.

3 Formalism:

Our main aim is to determine the collision integral of the transport Eq. 3. Once, we determine certain form of $C[f]$, we can proceed towards solving the differential equation.

⁵It is now possible to detect directly D mesons at LHC detectors like ALICE, see [16]

There are lots of approximations through which the integro-differential equation can be solved. Of course, under certain conditions, Eq. 3 can be reduced to the simple form:

$$\frac{\partial f(\mathbf{p}, t)}{\partial t} = -\frac{f - f_0}{\tau} \quad (4)$$

which is a useful first approximation. Here, f_0 is the equilibrium distribution function and τ is the relaxation time that determines the rate at which the fluctuations in the system drive it to a state of equilibrium again. In this form the equation is very easy to solve. But, our case is not so simple. We will deal with a more sophisticated approximation that leads to the Fokker-Planck equation [36].

To start with, we apply the Landau approximation which allows only soft scattering in the collision integral. If we define $w(\mathbf{p}, \mathbf{k})$ to be the rate of collisions which change the momentum of the HQ from \mathbf{p} to $\mathbf{p} - \mathbf{k}$, we have

$$\left[\frac{\partial f}{\partial t} \right]_{\text{collisions}} = \int d^3\mathbf{k} [w(\mathbf{p} + \mathbf{k}, \mathbf{k})f(\mathbf{p} + \mathbf{k}) - w(\mathbf{p}, \mathbf{k})f(\mathbf{p})]. \quad (5)$$

The second part of the integral corresponds to all those transitions that remove HQ from momentum \mathbf{p} to $\mathbf{p} - \mathbf{k}$, and therefore, represents a net loss to the distribution function. Likewise, the first part of the integral represents a net gain to the distribution function of HQ. With these, Eq. 3 becomes:

$$\frac{\partial f(\mathbf{p}, t)}{\partial t} = \int d^3\mathbf{k} [w(\mathbf{p} + \mathbf{k}, \mathbf{k})f(\mathbf{p} + \mathbf{k}) - w(\mathbf{p}, \mathbf{k})f(\mathbf{p})] \quad (6)$$

Eq. 6 is a linear equation in f . We can simplify it by assuming the previously discussed Landau approximation. Mathematically, this approximation amounts to assuming $w(\mathbf{p}, \mathbf{k})$ to fall off rapidly to zero with $|\mathbf{k}|$, i.e., transition probability function, $w(\mathbf{p}, \mathbf{k})$ is sharply peaked around $|\mathbf{k}| = 0$. Therefore, if we expand the integrand in the right hand side of Eq. 6 in powers of \mathbf{k} , we have

$$w(\mathbf{p} + \mathbf{k}, \mathbf{k})f(\mathbf{p} + \mathbf{k}) \approx w(\mathbf{p}, \mathbf{k})f(\mathbf{p}) + \mathbf{k} \cdot \frac{\partial}{\partial \mathbf{p}}(wf) + \frac{1}{2}k_i k_j \frac{\partial^2}{\partial p_i \partial p_j}(wf) \quad (7)$$

Retaining terms up to the second order only, we obtain Fokker-Planck equation [36]:

$$\frac{\partial f}{\partial t} = \frac{\partial}{\partial p_i} \left[A_i(\mathbf{p})f + \frac{\partial}{\partial p_j} [B_{ij}(\mathbf{p})f] \right] , \quad (8)$$

where the kernels are defined as the following:

$$A_i = \int d^3\mathbf{k} w(\mathbf{p}, \mathbf{k}) k_i , \quad (9)$$

and

$$B_{ij} = \frac{1}{2} \int d^3\mathbf{k} w(\mathbf{p}, \mathbf{k}) k_i k_j. \quad (10)$$

In the present formalism, we considered the elastic scattering of the HQ with the gluon, light quark and the corresponding anti-quarks. All these processes contribute to determine $w(\mathbf{p}, \mathbf{k})$ [36] and, in turn, the above defined kernels. Now, to explore the physical

significance of the A and B coefficients, let us consider $A_i = p_i \gamma(p)$ and $B_{ij} = D(p) \delta_{ij}$, which assume very low \mathbf{p} , i.e., the medium of QGP is isotropic to the HQ. If, in this limit, we neglect all the derivatives of A and B coefficients with momentum of HQ, Eq. 8 reduces to

$$\frac{\partial f}{\partial t} = \gamma \frac{\partial}{\partial \mathbf{p}} \cdot (\mathbf{p}f) + D \left[\frac{\partial}{\partial \mathbf{p}} \right]^2 f \quad (11)$$

The method of solution of this equation is elaborately discussed in [36]. Now, if we want to extend this formalism to the regime where the momentum of the HQ is no longer small, i.e., the particular kinematic domain where HQ becomes relativistic, obviously, we would like to know how the transport coefficients drag(γ) and diffusion(D) behave at high \mathbf{p} region. In order to do so we extrapolate the concept of isotropy to the higher momentum of HQ in such a way that only the first derivatives of the drag and diffusion coefficients are considered and the momentum dependence of A and B coefficients are encoded inside γ and D. Therefore, the Fokker-Planck equation, under this approximation, in Cartesian coordinate system becomes, [27]:

$$\begin{aligned} \frac{\partial f}{\partial t} &= C_1(p_x, p_y, t) \frac{\partial^2 f}{\partial p_x^2} + C_2(p_x, p_y, t) \frac{\partial^2 f}{\partial p_y^2} \\ &+ C_3(p_x, p_y, t) \frac{\partial f}{\partial p_x} + C_4(p_x, p_y, t) \frac{\partial f}{\partial p_y} \\ &+ C_5(p_x, p_y, t) f + C_6(p_x, p_y, t) \end{aligned} \quad (12)$$

where,

$$C_1 = D \quad (13)$$

$$C_2 = D \quad (14)$$

$$C_3 = \gamma p_x + 2 \frac{\partial D}{\partial p_T} \frac{p_x}{p_T} \quad (15)$$

$$C_4 = \gamma p_y + 2 \frac{\partial D}{\partial p_T} \frac{p_y}{p_T} \quad (16)$$

$$C_5 = 2 \gamma + \frac{\partial \gamma}{\partial p_T} \frac{p_x^2}{p_T} + \frac{\partial \gamma}{\partial p_T} \frac{p_y^2}{p_T} \quad (17)$$

$$C_6 = 0 \quad (18)$$

where the momentum, $\mathbf{p} = (\mathbf{p}_T, p_z) = (p_x, p_y, p_z)$. We numerically solve Eq. 12 [37] with the boundary conditions: $f(p_x, p_y, t) \rightarrow 0$ for $p_x, p_y \rightarrow \infty$ and the initial (at time $t = \tau_i$) momentum distribution of charm and bottom quarks are taken from MNR code [38]. It is evident from Eq. 12 that with the momentum dependent transport coefficients the FP equation becomes complicated.

It is possible to write down the solution of the FP equation in closed analytical form [39] in the special case of momentum independent drag and diffusion coefficients. To find out the solution f for momentum independent drag and diffusion coefficients we can consider the one-dimensional version of Eq. 11,

$$\frac{\partial f}{\partial t} = \gamma \frac{\partial}{\partial p} (pf) + D \frac{\partial^2 f}{\partial p^2}, \quad (19)$$

also called the Rayleigh's equation. For the initial condition $f(p, t = 0) = \delta(p - p_0)$, the solution of f is

$$f(p, t) = \left(\frac{\gamma}{2\pi D} (1 - e^{-2\gamma t}) \right)^{-1/2} \times \exp\left(-\frac{\gamma}{2D} \frac{(p - p_0 e^{-\gamma t})^2}{1 - e^{-2\gamma t}} \right) \quad (20)$$

However, Eq. 20 is solution for a very simplified scenario and we will study the momentum dependence of drag and diffusion coefficients and their effects on R_{AA} in the sections to come.

4 Drag Coefficients:

4.1 Elastic processes:

We need to evaluate the drag coefficient as a function of temperature and momentum of HQ. The expression to evaluate collisional drag can be written as [36]:

$$\begin{aligned} \gamma_{coll} &= \frac{1}{2E_p} \int \frac{d^3\mathbf{q}}{(2\pi)^3 2E_q} \int \frac{d^3\mathbf{q}'}{(2\pi)^3 2E_{q'}} \\ &\times \int \frac{d^3\mathbf{p}'}{(2\pi)^3 2E_{p'}} \frac{1}{\gamma_Q} \sum |M|^2 \\ &\times (2\pi)^4 \delta^4(p + q - p' - q') f'(\mathbf{q}) \left[1 - \frac{\mathbf{p} \cdot \mathbf{p}'}{p^2} \right] \end{aligned} \quad (21)$$

where $\mathbf{p}' = \mathbf{p} - \mathbf{k}$ and $\mathbf{q}' = \mathbf{q} + \mathbf{k}$. The scattering matrix elements are given explicitly in [40] where the t channel divergence occurring due to very soft gluon exchange has been shielded by replacing t in the denominator of matrix elements by $t - m_D^2$ in an ad hoc manner, where t is the Mandelstam variable and m_D is the thermal mass of gluon. However, the same problem can be approached from hard thermal loop (HTL) perturbation theory. The gluon propagator for t channel diagram is then replaced by HTL propagator. But, calculation of even the elastic matrix elements for HQs scattering with light quarks and gluons in this approach is very lengthy and radiative matrix elements are even clumsier. However, an outline of calculating collisional drag and diffusion coefficients in HTL perturbation theory approach is given for the interested readers in the Appendix. Here we proceed with the conventional process of shielding t channel divergence with the gluon thermal mass, m_D .

The integrations in Eq. 21 has been performed using the standard techniques [22, 23, 24, 36]. Results of the present calculation of drag coefficients are plotted with respect to momenta of charm and bottom (Fig. 1). We can observe that the momentum dependence of γ is non-negligible for the shown momentum range. The value of γ for charm due to collisional processes at $p = 5$ GeV is about 0.036 fm^{-1} which reduces to a value of 0.018 fm^{-1} at $p = 10$ GeV (can be compared with [41, 42, 43, 44] for example). In the inset, the drag coefficients of HQ's due to elastic collision are plotted in the lower

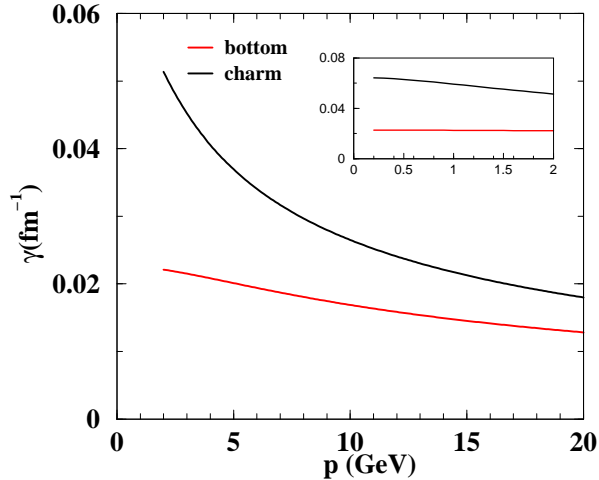


Figure 1: Drag coefficients of charm and bottom with their momentum at $T=300$ MeV assuming running strong coupling, $\alpha_s(T)$ and temperature dependent Debye screening mass, $m_D(T)$ for gluon, quark, and antiquark scattering.

momentum region, where the drag remains more or less constant with \mathbf{p} . Therefore, it is clear that had we taken the value of drag at low momentum and extrapolated that value to higher momentum, the final result would have been overestimated. The diffusion coefficient of HQ can be evaluated from Einstein relation $D = \gamma MT$. Later, it will be seen that the momentum dependence of transport coefficients of a high energy HQ will have considerable effects on the nuclear suppression factor, R_{AA} of HQ.

However, there are also radiative processes taking place in the medium. The radiative drag can be obtained in the present formalism by computing the radiative energy loss of a HQ passing through QGP. In the next section we will discuss the methods and intricacies of calculating the transport coefficients in radiative domain.

4.2 Radiative Processes:

It is already known that the two mechanisms of energy loss of heavy quarks are collisional and radiative energy loss. Though at low transverse momentum (p_T) region the collisional and radiative losses of HQs are comparable (see Fig. 5), the radiative one tends to dominate with increasing momentum. So it is worthwhile, after discussing about evaluation of collisional transport coefficients (drag, diffusion) within the ambit of $T = 0$ perturbative QCD (pQCD) [36] in the previous section, to contemplate on radiative processes and to inspect how pQCD approach can be utilized in finding out radiative transport coefficients.

It is well-known from QED that for high energies radiative energy loss becomes dominant [45]. Also the Hard Thermal Loop calculations in context of QCD show that the radiative energy loss contributes to same order of strong coupling as that of collisional loss [46]. The above discussions tempt one to infer that the observed large suppression of heavy quarks at RHIC is predominantly due to bremsstrahlung processes [24, 27], at least at high p_T ; but, as already said, the comparable values of energy losses in low momentum

region leaves an ample room for ambiguity in this statement particularly at ‘not-so-high’ p_T ($\sim 2 \text{ GeV}$) region.

Theoretical estimate of nuclear suppression factor (R_{AA}) for charm quarks in [27] shows ~ 4 times more suppression due to inclusion of radiation (Fig. 2) with same initial conditions. Inclusion of radiative processes leads to a good description of charm R_{AA} at RHIC energies. At LHC energy (2.76 TeV/A) the collisional energy loss due to hard

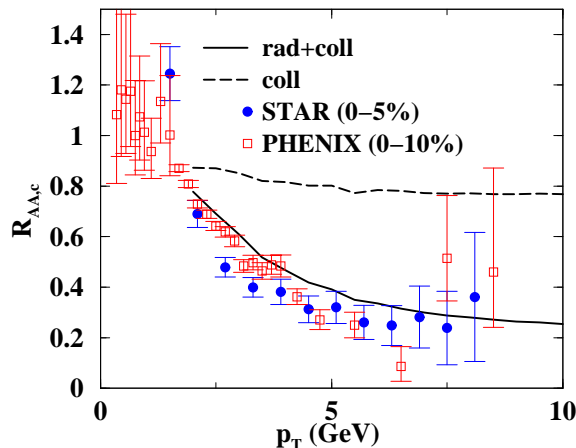


Figure 2: Suppression of transverse momentum of charm quarks in QGP as a function p_T

(momentum transfer $> 2 \text{ GeV}$) collisions could be about one-third of the total [28]. The rest may be attributed to radiative loss.

From the discussion on collisional transport coefficients we know that (collisional) drag is given by [36]

$$\gamma_{coll} = -\frac{1}{p} \left(\frac{dE}{dx} \right)_{coll}, \quad (22)$$

where p is the momentum of the probe. We employ a similar argument and relate radiative energy loss ($(dE/dx)_{rad}$) to inelastic drag (γ_{rad}) in the same way. The effective drag obtained is a summation of collisional and radiative parts. As energy loss is related with the transport properties like drag offered by the medium, we must concentrate on more and more accurate determination of radiative energy loss which will enable us to understand the properties of QGP.

The radiative energy loss in general has been studied in [47, 48, 49, 50, 51] incorporating Landau-Pomeranchuk-Migdal (LPM) effect [52], to be discussed later, due to multiple scattering. [53] treats the problem of radiative energy loss of HQs by building a model in scalar QCD approach. Attempts have been taken [24, 27, 29] to incorporate the formalism of [47], the Gyulassy-Wang potential model (GWPM), to compute the radiative energy loss of heavy quarks traveling through QGP. In stead of going to the energy loss in GWPM approach directly, we may try to acquire some familiarity with the model and the notations used for the description of it.

4.2.1 Gyulassy Wang Potential Model (GWPM) and radiation spectrum:

To analyze the multiple scattering and the induced gluon radiation in GWPM, certain simplifications have to be made. For example, [48] assumes static interaction between propagating parton and bath particles. This interaction is modelled by a static Debye screening potential. Now, it is possible to approximate the effective average random colour field produced by the bath particles by a potential provided the distance between two successive scatterers is large compared to colour screening length (μ^{-1}). The screened potential is given by:

$$\begin{aligned} V_{AA'}^a(\vec{q}) &= A_{AA'}^a(\vec{q})e^{-i\vec{q}\cdot\vec{x}} \\ &= gT_{AA'}^a\frac{e^{-i\vec{q}\cdot\vec{x}}}{\vec{q}^2 + \mu^2}, \end{aligned} \quad (23)$$

where μ is the colour screening mass, T^a are the generators corresponding to the representation of target partons at \vec{x} transferring (three) momentum \vec{q} and g is the coupling. The Feynman diagrams contributing to induced gluon radiation from a single quark-quark scattering is given in Fig. 3.

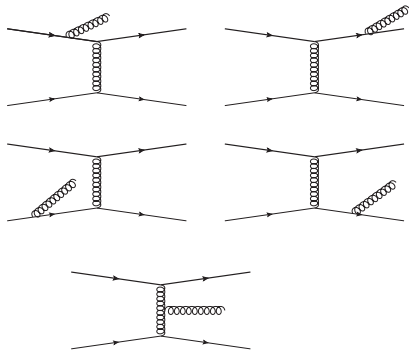


Figure 3: Feynman diagrams for gluon radiation from a single quark-quark (qq') scattering

The calculation of Feynman diagrams are done in light-cone co-ordinates [54] where light-cone representations of four-vectors are done in the following way,

$$\begin{aligned} p &= (p^+, p^-, p_\perp) \\ &= (p_0 + p_3, p_0 - p_3, p_\perp) \end{aligned} \quad (24)$$

In the potential model one can neglect radiation from the target lines (external lines appearing at the bottom of gluon propagator in Fig. 3) provided one decides to work in light cone gauge, $A^+ = 0$, for emitted gluon fields (For details see [55]). For radiation in the mid-rapidity region the celebrated Gunion-Bertsch distribution formula (GB formula) for soft gluon radiation [56] can be reproduced from this approach.

We now discuss the GB formula and recent attempts to generalize ⁶it because we will see that this formula and/or its generalizations will play a significant role in finding out the energy loss due to gluon emission of quarks. The early attempts of generalizing GB

⁶Interested readers are referred to the Appendix for other such very recent endeavors.

formula [57, 58, 59] consider the general $gg \rightarrow ggg$ matrix element elegantly written by [60] and factoring out the elastic $gg \rightarrow gg$ scattering amplitude to obtain the distribution of emitted gluon ($\sim |M_{gg \rightarrow ggg}|^2 / |M_{gg \rightarrow gg}|^2$). We can write the following form of gluon distribution [59], (for details see Appendix of [59])

$$\begin{aligned} \frac{dn_g}{d^2k_\perp d\eta} &= \left[\frac{dn_g}{d^2k_\perp d\eta} \right]_{GB} \left[\left(1 + \frac{t}{2s} + \frac{5t^2}{2s^2} - \frac{t^3}{s^3} \right) \right. \\ &\quad - \left. \left(\frac{3}{2\sqrt{s}} + \frac{4t}{s\sqrt{s}} - \frac{3t^2}{2s^2\sqrt{s}} \right) k_\perp \right. \\ &\quad \left. + \left(\frac{5}{2s} + \frac{t}{2s^2} + \frac{5t^2}{s^3} \right) k_\perp^2 \right], \end{aligned} \quad (25)$$

where η is the rapidity of the radiated gluon, the subscript GB has been used to indicate the gluon spectrum obtained using the approximation considered in [56] (see also [61]) which is generally given by,

$$\left[\frac{dn_g}{d^2k_\perp d\eta} \right]_{GB} = \frac{C_A \alpha_s}{\pi^2} \frac{q_\perp^2}{k_\perp^2 [(\vec{k}_\perp - \vec{q}_\perp)^2 + m_D^2]}, \quad (26)$$

where $m_D = \sqrt{\frac{2\pi}{3} \alpha_s(T) \left(C_A + \frac{N_F}{2} \right)}$, T , is the thermal mass of the gluon [62, 63], N_F is the number of flavours contributing in the gluon self-energy loop, $C_A = 3$ is the Casimir invariant for the SU(3) adjoint representation, α_s is the temperature-dependent strong coupling [64], k_\perp is the transverse momentum of the emitted gluon and q_\perp is the transverse momentum transfer. In general, one introduces the thermal mass in the denominator of Eq. 26 to shield the divergence arising from collinearity (*i.e.* when $\vec{k}_\perp = \vec{q}_\perp$) of emitted gluon. But, for the present case Eq. 25 is written under the assumption that $\vec{q}_\perp \gg \vec{k}_\perp$; and hence, there is no need to write the m_D^2 factor in GB spectrum.

Now, we must consider multiple scattering encountered by incoming particles, too. The many body effect due to presence of medium results in interference of scattering amplitudes. This interference effect is called LPM effect [52]. LPM effect is discussed in QED domain in [65]. LPM suppression can be understood in a qualitative manner as an interplay between two time scales, the formation time (τ_f) and the scattering time (τ_{sc}). τ_f is the time needed for the emission of the induced gluon. Actually, τ_f determines the time span after which a radiation can be separately identified from the parent parton from which the radiation is being given off. Now, a collision just before formation of the gluon results in suppression of the radiation. This destructive interference is called LPM effect and in the next section we will see that it puts a constraint on the phase space of the emitted gluon. If k_0 is the energy of the emitted (soft) gluon and k_\perp is its transverse momentum, then formation time $\tau_f \sim \frac{2k_0}{k_\perp^2}$ [48]. When this τ_f is much less than collision time *i.e.*, separation between two scattering centres, L , then the intensity of radiation is additive and *Bethe-Heitler(BH) limit* is reached. In the *factorization limit*, $L \ll \tau_f$, the interference in radiation amplitude takes place and LPM effect dominates.

After this brief discussion on possible effects of multiple scattering, emitted gluon distribution due to multiple scattering in terms of that due to single scattering can be

written as [48]:

$$\frac{dn_g^{(m)}}{d^2k_\perp d\eta} = C_m(k) \frac{dn_g^{(1)}}{d^2k_\perp d\eta}, \quad (27)$$

where ‘ m ’ stands for multiple scattering and ‘1’ stands for single scattering. C_m is called radiation formation factor characterizing the interference pattern due to multiple scattering. Naturally, in the BH limit, $C_m \approx m$, *i.e.* the scatterings add up to give the resultant intensity with no interference pattern. On the other hand, the factorization limit gives [48, 49],

$$\begin{aligned} C_m(k) &\approx \frac{8}{9}[1 - (-1/8)^m] && \text{for quarks} \\ &\approx 2(1 - 1/2^m) && \text{for gluons} \end{aligned} \quad (28)$$

Eq. 28 shows that the interference effect due to many multiple scatterings for quarks leaves corresponding radiation spectrum a factor of $\sim 8/9$ of that due to single scattering. It can also be checked that the gluon intensity radiated by gluon jet is $9/4$ times higher than that radiated by quark jets in multiple scattering. Thus, the LPM effect in QCD depends on colour representation due to non-abelian nature of the problem under discussion.

4.2.2 Energy Loss of light particles in GWPM:

The energy loss in potential model can be evaluated by integrating over the transverse momentum and rapidity of emitted gluon. The phase space is, of course, constrained by LPM effect due to multiple scattering. The multiple scattering is implemented through the differential change of the factor C_m with number of scattering m , $\frac{dC_m}{dm}$, which can be approximated as a θ -function [48]. Also, the emitted gluon must have energy less than that of the parent parton. So the energy loss formula implementing the energy constraint gives:

$$\begin{aligned} \Delta E_{rad} &= \frac{E_{m+1} - E_m}{m} \\ &= \int d^2k_\perp d\eta \frac{dn_g}{d^2k_\perp d\eta} k_0 \frac{C_{m+1} - C_m}{m} \theta(E - k_\perp \cosh\eta) \\ &= \int d^2k_\perp d\eta \frac{dn_g}{d^2k_\perp d\eta} k_0 \frac{dC_m}{dm} \theta(E - k_\perp \cosh\eta) \\ &\sim \int d^2k_\perp d\eta \frac{dn_g}{d^2k_\perp d\eta} k_0 \theta(\tau_{sc} - \tau_F) \theta(E - k_\perp \cosh\eta) \end{aligned} \quad (29)$$

where E is the energy of the parent parton and $k_0 = k_\perp \cosh\eta$, E_{m+1} denotes energy loss in $(m+1)^{th}$ collision and E_m is that in m^{th} collision. The first θ -function involving scattering time τ_{sc} [66] gives a lower limit of k_\perp , *i.e.* $k_\perp > \Lambda \cosh\eta$. The second θ -function yields, $k_\perp < E/\cosh\eta$. Utilizing Eq. 29, [59] compares the energy loss (Fig. 4) of a gluon jet passing through gluonic plasma obtained by generalized GB formulae given in [57, 58, 59]. We will see how Eq. 29 can be employed to find out HQ energy loss in the next section.

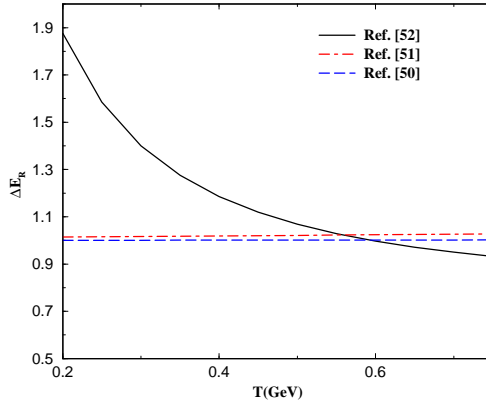


Figure 4: (Color online) Temperature variation of ΔE_R , *i.e.* ΔE normalized by the corresponding value obtained from GB approximation, of a 15 GeV gluon due to traversal of 4 fm in a gluonic heat bath. Solid (dashed) line indicates result for the gluon spectrum obtained in [59] ([57]). The dot-dashed line stands for the results for the gluon spectrum of [58].

4.2.3 Energy Loss of HQs and radiative drag:

While calculating the radiative energy loss of HQs [53] takes the GB distribution for small and moderate x and for mass $m \neq 0$. The distribution, so obtained, can be shown to yield GB distribution when $x \ll 1$ and when $m = 0$. Whereas, [24, 27] use the original GB distribution formula weighted by a radiative suppression factor, called ‘Dead-cone’ factor, originating due to mass of HQs. Since dead-cone factor plays an important role in radiative energy loss of heavy quarks, we will pause here to spend some words on Dead-cone effect in QCD [68] and its generalizations.

The dead cone suppression obtained in [68] actually has an analogy with radiated power distribution of a non-relativistic, accelerating charge particle. The average power radiated per unit solid angle is given by [69]:

$$\frac{dP}{d\Omega} \propto |\dot{\vec{\beta}}|^2 \sin^2\theta, \quad (30)$$

where θ is the angle between acceleration $\dot{\vec{\beta}}$ of the particle and the direction of propagation of radiation, \vec{n} . This is a simple $\sin^2\theta$ behaviour showing no radiation at $\theta = 0$ (or $n\pi, n \in \mathbb{Z}$). It can be shown [70] that the behaviour of Eq. 30 is, indeed, similar to what one gets for conventional dead cone [68]. Qualitatively speaking, it is hard to cause a deceleration of a high energy heavy quarks along their directions of motion; and this is why the bremsstrahlung radiation is suppressed along this direction (see Fig. 24). Indeed, the distribution of radiated gluons emanating from HQs are shown to be related to those from light quarks (LQs) by the following formula [68] (for small radiation angle θ):

$$dP_{HQ} = \left(1 + \frac{\theta_0^2}{\theta^2}\right)^{-2} dP_{LQ}, \quad (31)$$

where $\theta_0 = m/E$; m is the mass and E is the energy of heavy quark. It is worth noting that when $E \rightarrow \infty$, the radiation from HQs converges with that of LQs. However, there are some very recent developments in generalizing the dead-cone effect either from $Qq \rightarrow Qqg$ matrix element or assuming effects of off-shellness of quarks which, after being produced, take some time to become on-shell. The details may be seen in the Appendix.

The radiative transport coefficients like drag, diffusion have been evaluated in [24, 27] employing potential approach. The radiative drag coefficient can be obtained by finding out the radiative energy loss of HQs passing through medium. The GB spectrum for emitted gluon, weighted by the dead-cone factor and the energy of gluon $k_0 (= k_\perp \cosh \eta)$, is integrated over the transverse momentum (k_\perp) and rapidity (η) of the emitted gluon. As already stated, the lower and upper limits of k_\perp has been obtained from the θ -functions of Eq. 29. The average energy loss per collision, ΔE_{rad} , can be written with the help of Eq. 29,

$$= \langle n_g k_0 \rangle = \int d\eta d^2 k_\perp \frac{dn_g}{d\eta d^2 k_\perp} \times k_0 \Theta(\tau_{sc} - \tau_F) \Theta(E - k_\perp \cosh \eta) F_{DC}^2, \quad (32)$$

where the formation time of the emitted gluon [48], $\tau_F = (C_A/2C_2) 2 \cosh \eta/k_\perp$, and $C_A/2C_2 = N^2/(N^2 - 1)$ for quarks with $C_2 = C_F = 4/3$. Dead-cone factor of Eq. 31 (dP_{HQ}/dP_{LQ}) can be written in the following way, provided one replaces $k_\perp/k_0 \sim \sin \theta \sim \theta$ for small θ ,

$$F_{DC}^2 = \left(\frac{k_\perp^2}{k_0^2 \theta_0^2 + k_\perp^2} \right)^2, \quad (33)$$

dE/dx can be obtained if one multiplies ΔE_{rad} with Λ , which can be obtained from [66]. Drag (γ) and diffusion ($D = \gamma m T$) coefficients in [27] are functions of momentum as well as temperature. The effective drag can be obtained by adding collisional and radiative drags, $\gamma_{eff} = \gamma_{coll} + \gamma_{rad}$. The momentum dependence of the drag coefficient of the charm quark propagating through the QGP is displayed in Fig. 5 for $T = 300$ MeV. For $p_T \sim 2$ GeV of charm quarks the collisional and radiative contributions tend to merge with each other. However, it is interesting to note the dominance of radiative drag in Fig. 5 over its collisional counterpart for higher momentum.

5 Space-Time Evolution

Once we know the total drag (γ_{eff}) and diffusion (D_{eff}) coefficients, we need the initial conditions for both the HQ and the QGP background which is also evolving with time following,

$$\partial_\mu T^{\mu\nu} = 0 \quad (34)$$

where, $T^{\mu\nu} = (\epsilon + P)u^\mu u^\nu - g^{\mu\nu} P$, is the energy momentum tensor for ideal fluid, ϵ is the energy density, P is the pressure and u^μ is the hydrodynamic four velocity, and $g^{\mu\nu}$ is the metric tensor. We will solve this equation for longitudinal expansion assuming boost invariance along the z direction [71]. It is expected that the central rapidity region of the system formed after nuclear collisions at RHIC and LHC energy is almost net baryon

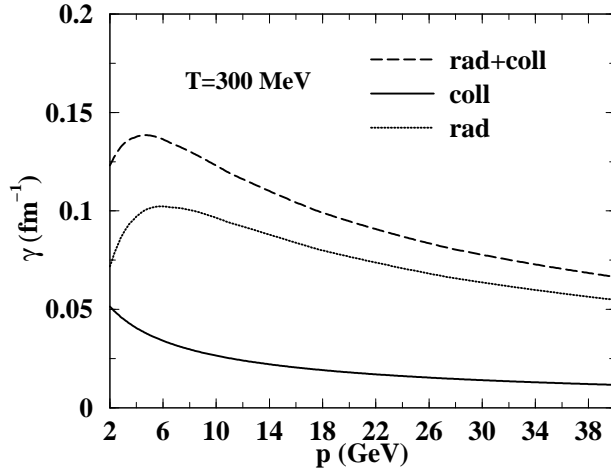


Figure 5: Drag coefficients of charm assuming running strong coupling, $\alpha_s(T)$ and temperature dependent Debye screening mass, $m_D(T)$ due to its interaction with thermal gluons, quarks, and antiquarks.

free. Therefore, the equation governing the conservation of net baryon number need not be considered here. Under this circumstance Eq. 34 reduces to:

$$\frac{\partial \epsilon}{\partial \tau} + \frac{\epsilon + P}{\tau} = 0 \quad (35)$$

To solve Eq. 35, we use the relation $P = c_s^2 \epsilon$, where c_s is the velocity of sound and τ is time. With this we arrive at the relation,

$$\epsilon \tau^{1+c_s^2} = C \quad (36)$$

where C is a constant. For the ideal equation of state, $c_s^2 = \frac{1}{3}$, the above Eq. reads $\epsilon \tau^{\frac{4}{3}} = C$. In terms of temperature this relation can be written as $\tau T^3 = C$.

The total amount of energy dissipated by a heavy quark in the expanding QGP depends on the path length it traverses. Each parton traverses different path length which depends on the geometry of the system and on the point where its is created. The probability that a parton is produced at a point (r, ϕ) in the plasma depends on the number of binary collisions at that point which can be taken as [72]:

$$P(r, \phi) = \frac{2}{\pi R^2} \left(1 - \frac{r^2}{R^2}\right) \theta(R - r) \quad (37)$$

where R is the nuclear radius. It should be mentioned here that the expression in Eq. (37) is an approximation for the collisions with zero impact parameter. A very high energy parton created at (r, ϕ) in the transverse plane propagates a distance $L = \sqrt{R^2 - r^2 \sin^2 \phi} - r \cos \phi$ in the medium provided its direction remains unaltered. In the present work we use the following equation for the geometric average of the integral involving drag coefficient

$$\Gamma = \frac{\int r dr d\phi P(r, \phi) \int^{L/v} d\tau \gamma(\tau)}{\int r dr d\phi P(r, \phi)}, \quad (38)$$

where v is the velocity of the propagating partons. Similar averaging has been performed for the diffusion coefficient, too. For a static system the temperature dependence of the drag and diffusion coefficients of the heavy quarks enter via the thermal distributions of light quarks and gluons through which it is propagating. However, in the present scenario the variation of temperature with time is governed by the equation of state or velocity of sound of the thermalized system undergoing hydrodynamic expansion. In such a scenario the quantities like Γ (Eq. 38) and hence the HQ suppression becomes sensitive to c_s .

6 Initial Conditions and Nuclear Modification Factor

In order to solve Eq. 12, the initial distribution functions, $f_{in}(p_T, t)$ for charm and bottom quarks have been supplied from the well known MNR code [38]. The ratio between the solution of Fokker-Planck Equation at the transition temperature, $T_c = 175$ MeV and the initial distribution function of HQ is the required nuclear modification factor, R_{AA} of open HQ. But, in order to compare results from the present formalism with experimental data from RHIC and LHC we need to have R_{AA} of non-photonic single electron originating from the decays of D and B mesons.

Therefore, the hadronization of charm and bottom quarks to D and B mesons respectively are done by using Peterson fragmentation function [73]:

$$f(z) \propto \frac{1}{[z[z - \frac{1}{z} - \frac{\epsilon_Q}{1-z}]^2]} \quad (39)$$

where, z is the fraction of momentum carried by the hadrons, ϵ_Q is 0.05 for charm and $(m_c/m_b)^2\epsilon_Q$ for bottom where $m_c(m_b)$ is the mass of charm(bottom). One may use different kinds of available fragmentation functions, but the final result will not be sensitive to the choice of $f(z)$. In point of fact, describing hadronization has always been a formidable task because the hadron bound states are non-perturbative in nature. The fragmentation scheme is a popular method to deal with hadronization. For more relevant information interested readers are referred to [74], which discusses coalescence model, a hadronization formulation based on recombination of heavy flavours.

Both the final solution of FP Equation and the initial distribution of HQ are convoluted with the above fragmentation function (Eq. 39) and their ratio will give R_{AA} of D and B mesons. The final and initial distribution functions are obtained for the single electrons originated from the decays of D and B mesons and the final nuclear modification factor is:

$$R_{AA}^{D(B) \rightarrow e} = \frac{f^{D(B) \rightarrow e}(p_T, T_c)}{f^{D(B) \rightarrow e}(p_T, T_i)} \quad (40)$$

Now, once we know how to determine R_{AA} , we will compare our results with the RHIC and LHC data. In the process of doing so we will study the effects of the equation of state on the nuclear suppression of heavy flavours in quark gluon plasma and estimate the initial entropy density of the QGP formed at the RHIC. For this purpose, the experimental data on the charged particle multiplicity and the nuclear suppression of single electron spectra originating from the semi-leptonic decays of D and B mesons have been employed. We

have used inputs from lattice QCD (LQCD) to minimize the model dependence of the results.

The initial entropy density and the thermalization time (τ_i) for the QGP can be constrained to the measured (final) multiplicity by the following relation [75] which is boost invariant:

$$s_i \tau_i = \kappa \frac{1}{A_\perp} \frac{dN}{dy} \quad (41)$$

where A_\perp is the transverse area of the system which can be determined from the collision geometry and κ is a known constant (=3.7 for massless Bosons).

Equation of state (EoS), which is taken as $P = c_s^2 \epsilon$ for almost baryon free QGP expected at RHIC energy, also has its own role to play in the space-time evolution of QGP. This sound velocity squared appearing in the EoS shows a significant variation with temperature in LQCD calculations (fig.6).

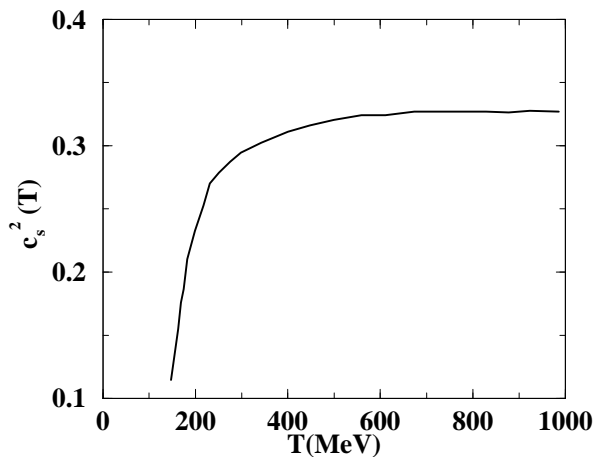


Figure 6: Velocity of sound squared as a function temperature [7]

In Fig. 10 we show the variation of T_i with c_s^2 obtained by constraints imposed by the experimental data on R_{AA} and dN/dy . The value of T_i varies from 210 to 300 MeV depending on the value of c_s . It is interesting to note that the lowest value of T_i obtained from the present analysis is well above the quark-hadron phase transition temperature, indicating the fact that the system formed in Au+Au collisions at $\sqrt{s_{NN}} = 200$ GeV might be formed in the partonic phase.

The data for R_{AA} of D^0 from ALICE are also contrasted with our results (see fig.11) when $c_s^2 = 1/3$ [11]. The EoS sets the expansion time scale for the system as $\tau_{exp} \sim [(1/\epsilon)d\epsilon/d\tau]^{-1} \sim \tau/(1+c_s^2)$ indicating the fact that lower value of c_s makes the expansion time scale longer *i.e.* the rate of expansion slower. This issue is further discussed in details in [76].

The result of R_{AA} , where the EoS contains temperature dependent c_s^2 , is displayed in Fig. 7. Here, the experimentally measured suppression [12, 13] has been reproduced reasonably well at $T_i = 250$ MeV and $\tau_i = 0.83$ fm/c. The T_i value, however, may increase if we take into account the transverse expansion because the inflation dilutes the medium.

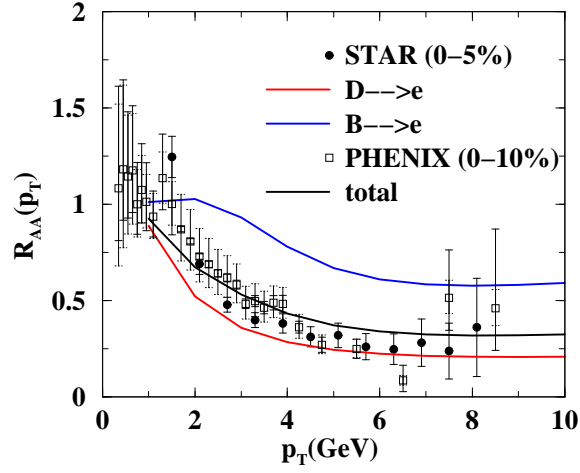


Figure 7: (colour online) Variation of R_{AA} with p_T for the space time evolution with initial condition $T_i = 250$ MeV and $\tau_i = 0.84$ fm/c and the EoS which includes the variation of c_s with T .

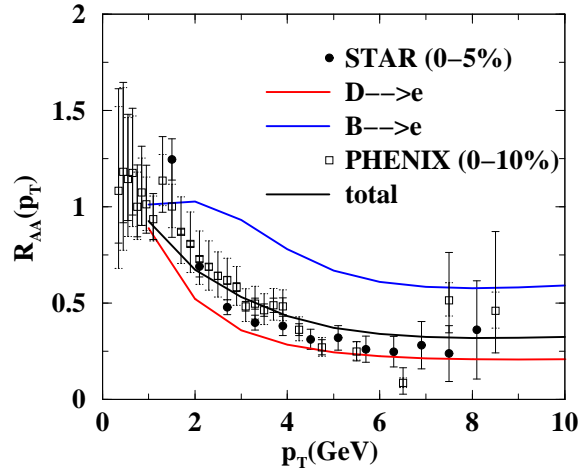


Figure 8: (colour online) Variation of R_{AA} with p_T for for $c_s^2 = 1/3$ and $T_i = 300$ MeV.

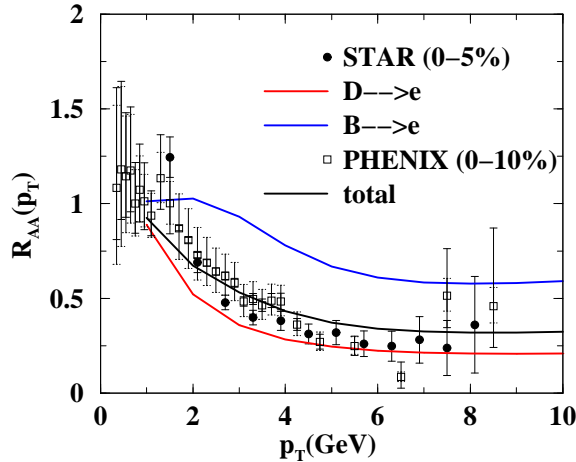


Figure 9: (colour online) Variation of R_{AA} with p_T for $c_s^2 = 1/5$ and $T_i = 210$ MeV.

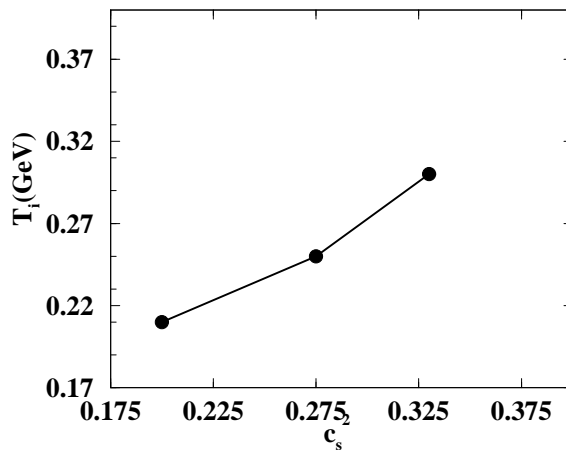


Figure 10: The variation of T_i with c_s^2 for fixed dN/dy .

Now, we know that larger c_s makes the QGP life time smaller leading to lesser suppression of HQ propagating through QGP for a shorter time. Therefore, when the value of c_s^2 is taken to be $1/3$, *i.e.* the highest possible value, the maximum value of T_i , which is in this analysis 300 MeV, will be reached. The value of s_i is $\sim 59/\text{fm}^3$ at T_i . These values of T_i and s_i are considered as the highest values of them admitted by the data. The result for the highest value of c_s^2 is illustrated in Fig. 8. Likewise, the result of R_{AA} in the case when $c_s^2 = 1/5$ is depicted in Fig. 9. In this case, the data is well reproduced at $T_i = 210$ MeV and $s_i \sim 19.66/\text{fm}^3$.

Now, it is expected that the central rapidity region of the system formed after nuclear collisions at high energy RHIC and LHC run is almost net baryon free. Therefore, the equation governing the conservation of net baryon number need not be considered here and all our calculations are valid for zero baryonic chemical potential ($\mu_B = 0$) cases. One may be interested in calculating transport coefficients in $\mu_B \neq 0$ case which may be of

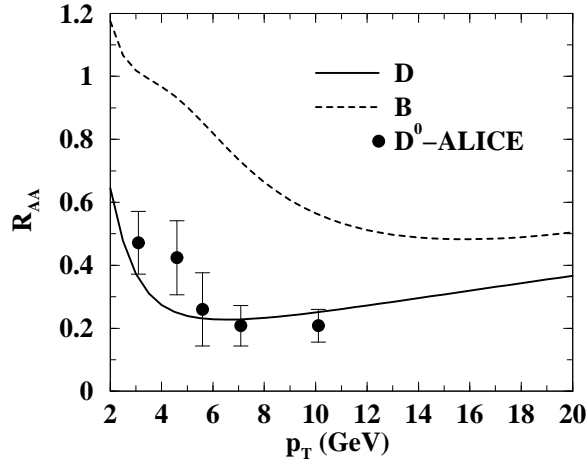


Figure 11: R_{AA} as a function of p_T for D and B mesons at LHC. Experimental data taken from [16].

importance in low energy RHIC run [77, 78] and GSI-FAIR [79]. This aspect is discussed in the next section.

7 Drag and diffusion at finite baryonic chemical potential

The nuclear collisions at low energy RHIC run [77, 78] and GSI-FAIR [79] is expected to create a thermal medium with large baryonic chemical potential (μ_B) and moderate temperature (T). So the effect of baryonic chemical potential (μ_B) on the transport coefficients of HQ should also been taken into account. Both the temperature (T) and quark chemical potential, μ ($= \mu_B/3$) dependence of drag enter through the thermal distribution.

The variation of the drag coefficients of charm quarks (because of its interactions with quarks and anti-quarks) with the baryonic chemical potential for different T are displayed in Fig. 12. The drag coefficient for the process : $Qg \rightarrow Qg$ is $\sim 8.42 \times 10^{-3} \text{ fm}^{-1}$ ($1.86 \times 10^{-2} \text{ fm}^{-1}$) for $T = 140 \text{ MeV}$ (190 MeV) (not shown in Fig. 12). The dependence of the drag and diffusion coefficients on temperature (T) and baryonic chemical potential (μ) may be understood as follows: As already discussed, the drag may be defined as the thermal average of the momentum transfer, $p - p'$, weighted by the square of the invariant transition amplitude for the reactions $qQ \rightarrow qQ$, $Q\bar{q} \rightarrow Q\bar{q}$ and $gQ \rightarrow gQ$. The average momentum of the quarks of the thermal bath increases with both T and μ . The increase in average momenta enables the thermal quarks to transfer larger momentum; and thus enhances the drag coefficient. This trend is clearly observed in the results displayed in Fig. 12 for charm quark. The drag due to the process $Qq \rightarrow Qq$ is larger than the $Q\bar{q} \rightarrow Q\bar{q}$ interaction because for $\mu \neq 0$. The Q propagating through the medium interacts with more q than \bar{q} at a given μ ; and so, zero chemical potential case yields the

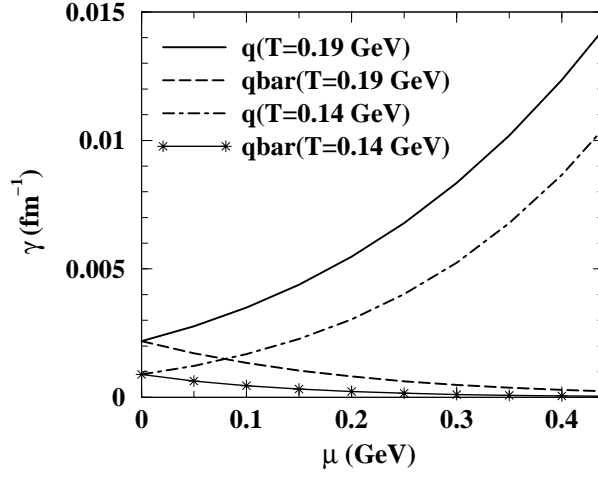


Figure 12: Variation of the drag coefficient of charm quark due to its interactions with light quarks and anti-quarks as a function of μ for different temperatures.

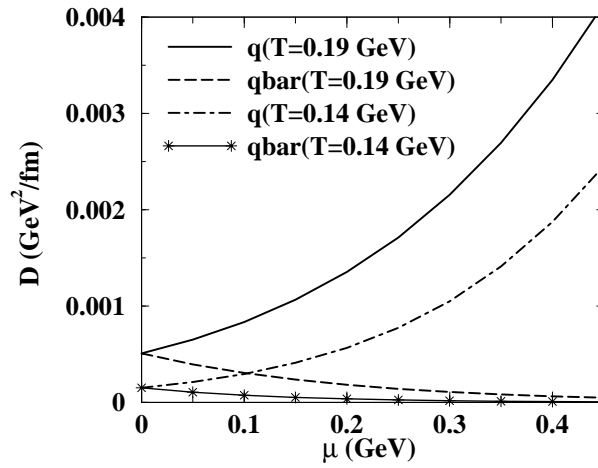


Figure 13: Variation of the diffusion coefficient of charm quark due to its interactions with light quarks and anti-quarks as a function of μ for different temperatures.

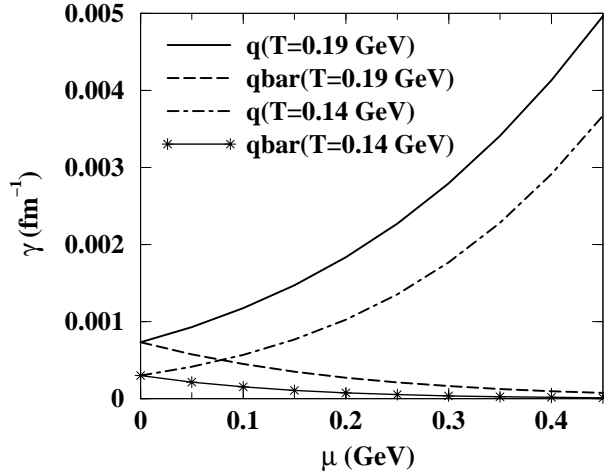


Figure 14: Same as Fig. 12 for bottom quark

same contributions from quarks and anti-quarks.

Similarly, it may be argued that the diffusion coefficient, which involves the square of the momentum transfer, should also increase with T and μ as observed in Fig. 13. The diffusion coefficient for charm quarks due to its interaction with gluons is given by $\sim 1.42 \times 10^{-3} \text{ GeV}^2/\text{fm}$ ($4.31 \times 10^{-3} \text{ GeV}^2/\text{fm}$) for $T = 140 \text{ MeV}$ (190 MeV). The drag and diffusion coefficients for bottom quarks are displayed in Figs. 14 and 15 respectively, showing qualitatively similar behaviour with that of charm quarks. The drag coefficients for bottom quarks due to the process $Qg \rightarrow Qg$ is given by $\sim 3.15 \times 10^{-3} \text{ fm}^{-1}$ and $6.93 \times 10^{-3} \text{ fm}^{-1}$ at $T = 140 \text{ MeV}$ and 190 MeV respectively. The corresponding diffusion coefficients are $\sim 1.79 \times 10^{-3} \text{ GeV}^2/\text{fm}$ and $5.38 \times 10^{-3} \text{ GeV}^2/\text{fm}$ at $T=140 \text{ MeV}$ and 190 MeV respectively. The chemical potential dependent drag and diffusion coefficients will be used later to find out the nuclear suppression of the heavy flavours for low energy RHIC experiments.

8 Nuclear Suppression in Baryon Rich QGP

For low energy collisions, the collisional energy loss of heavy quarks dominate over the radiation because HQs are produced with very low momentum. Moreover, the thermal production of charm and bottom quarks can be ignored in the range of temperature and baryonic chemical potential considered in the low energy nuclear collisions. Therefore, one can apply the FP equation for non-zero μ_B for the description of HQ evolution in the baryon rich QGP. The drag and diffusion coefficients are, now, functions of both the thermodynamical variables: μ_B and T .

The colliding energy ($\sqrt{s_{NN}}$) dependence of the chemical potential can be obtained from the parametrization of the experimental data on hadronic ratios as [80] (see also [81]),

$$\mu_B(s_{NN}) = a(1 + \sqrt{s_{NN}}/b)^{-1} \quad (42)$$

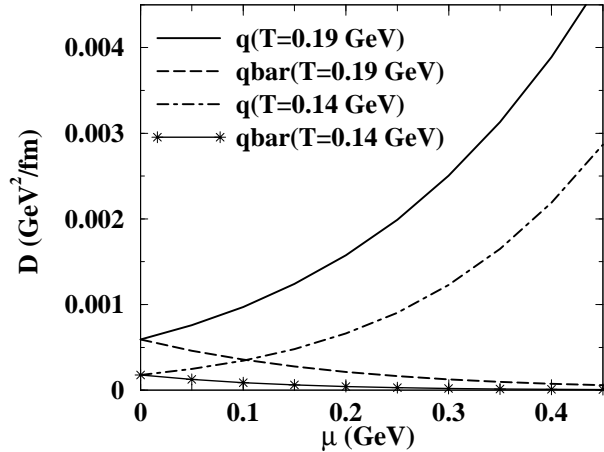


Figure 15: Same as Fig. 13 for bottom quark.

where $a = 0.967 \pm 0.032$ GeV and $b = 6.138 \pm 0.399$ GeV. The parametrization in Eq. 42 gives the values of μ_B . The chemical potential of the system, at mid rapidity, decreases with respect to the colliding energy as shown in Fig. 16. So the composition of matter produced at LHC and RHIC is different from the matter produced at low energy RHIC run. At LHC and RHIC the matter produced at the mid rapidity is almost net baryon free, whereas the matter produced at the low energy RHIC run are dominated by baryons at the mid rapidity.

To take care of this extra baryons we need to solve the energy-momentum conservation equation constrained by the baryon-number conservation equation. i.e. we simultaneously solve

$$\partial_\mu T^{\mu\nu} = 0 \quad (43)$$

and

$$\partial_\mu n_B^\mu = 0 \quad (44)$$

in (1+1) dimension with boost invariance along the longitudinal direction [71]. In the baryon-number conservation equation $n_B^\mu = n_B u^\mu$ is the baryonic flux and u^μ is the hydrodynamic four velocity. The initial baryonic chemical potential carried by the quarks $\mu (= \mu_B/3)$ are shown in Table 1 for various $\sqrt{s_{NN}}$ under consideration.

Table 1: The values center of mass energy $\sqrt{s_{NN}}$, dN/dy , initial temperature (T_i) and quark chemical potential - used in the present calculations.

$\sqrt{s_{NN}}(\text{GeV})$	$\frac{dN}{dy}$	$T_i(\text{MeV})$	$\mu(\text{MeV})$
39	617	240	62
27	592	199	70
17.3	574	198	100
7.7	561	197	165

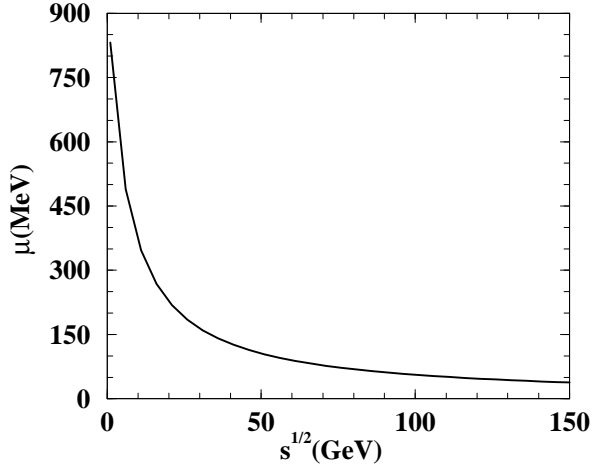


Figure 16: Variation of μ_B with respect to the $\sqrt{s_{NN}}$.

Multiplicities for various $\sqrt{s_{NN}}$ have been calculated from the Eq. below [82];

$$\frac{dN}{dy} = \frac{dn_{pp}}{dy} \left[(1-x) \frac{\langle N_{part} \rangle}{2} + x \langle N_{coll} \rangle \right] \quad (45)$$

N_{coll} is the number of collisions and contribute x fraction to the multiplicity dn_{pp}/dy measured in pp collision. The number of participants, N_{part} contributes a fraction $(1-x)$ to dn_{pp}/dy , which is given by

$$\frac{dn_{pp}}{dy} = 2.5 - 0.25 \ln(s) + 0.023 \ln^2(s) \quad (46)$$

The values of the number of participants, N_{part} , and number of collisions, N_{coll} , are estimated for $(0 - 5\%)$ centrality's by using Glauber Model [83]. The value of x depends very weakly on $\sqrt{s_{NN}}$ [84], in the present work we have taken $x = 0.1$ for all the colliding energies considered herein.

We need the initial heavy quark momentum distributions for solving the FP equation at finite baryonic chemical potential. For low collision energy rigorous QCD based calculations for heavy flavour production at proton-proton collision is not available. In the present work the initial HQ distribution is obtained from pQCD calculation [40, 85] for the processes: $gg \rightarrow Q\bar{Q}$ and $q\bar{q} \rightarrow Q\bar{Q}$. To highlight the effect of non-zero baryonic chemical potential we evaluate R_{AA} for $\mu = 200$ MeV and $\mu = 0$ for a given $T_i = 200$ MeV. The results are shown in Fig. 17 representing the combined effects of temperature and baryon density on the drag and diffusion coefficients. The drag coefficient of the heavy quarks due to its interaction with quarks is larger than that owing to its interactions with the anti-quarks (Fig.12), resulting in larger suppression in the former case than the latter. The net suppression of the electron spectra from the Au+Au collisions compared to p+p collisions is affected by quarks, anti-quarks and gluons. The results for net suppressions are displayed for $\mu = 200$ MeV (dashed line) and $\mu = 0$ (with asterisk). The experimental detection of the non-zero baryonic effects will shed light on the net baryon density

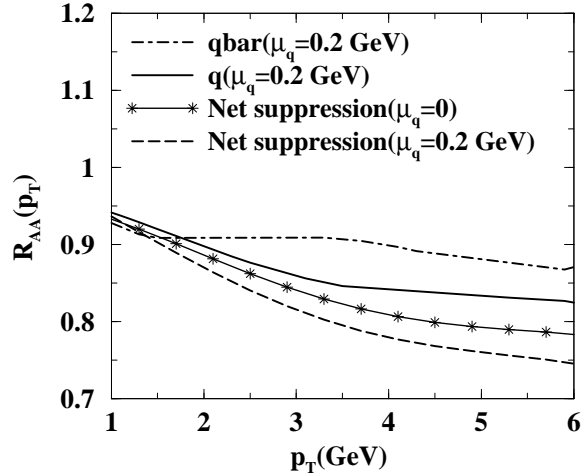


Figure 17: The nuclear suppression factor R_{AA} as a function of p_T due to the interaction of the charm quark (solid line) and anti-quark (dashed-dot line) for $\mu = 200$ MeV. The net suppressions including the interaction of quarks, anti-quarks and gluons for $\mu = 200$ MeV (dashed line) and $\mu = 0$ (with asterisk) are also shown.

(and hence baryon stopping). However, whether the effects of non-zero baryonic chemical potential is detectable or not will depend on the overall experimental performance.

The results for R_{AA} are shown in Fig. 18 for various $\sqrt{s_{NN}}$ with inputs from Table 1. We find that at large p_T the suppression is similar for all energies colliding energies considered in the present work. This is because the collisions at high $\sqrt{s_{NN}}$ are associated with large temperature but small baryon density at mid-rapidity- which is compensated by large baryon density and small temperature at low $\sqrt{s_{NN}}$ collisions. Low p_T particles predominantly originate from low temperature and low density part of the evolution where drag is less and so is the nuclear suppression.

In our earlier work [22] we have evaluated the R_{AA} for non-photon single electron spectra resulting from the semileptonic decays of hadrons containing heavy flavours. We observed that the data from RHIC collisions at $\sqrt{s_{NN}} = 200$ GeV are well reproduced by enhancing the pQCD cross sections by a factor 2 and with an equation of state $P = \epsilon/4$ for collisional loss. In the same spirit we evaluate R_{AA} with doubled pQCD cross section and keeping all other quantities same (Fig. 19). The results in Fig. 19 show stronger suppression as compared to the results displayed in Fig. 18, however it is similar for all the colliding energies considered in the present article.

9 Glimpses of Elliptic Flow

However, apart from the nuclear suppression factor R_{AA} , another experimental observable of heavy flavour, elliptic flow (v_2), can be studied within the framework of Fokker-Planck equation. The elliptic flow (v_2) of the produced particles has been considered as one of the most promising signals for the early thermalization of the matter formed in heavy

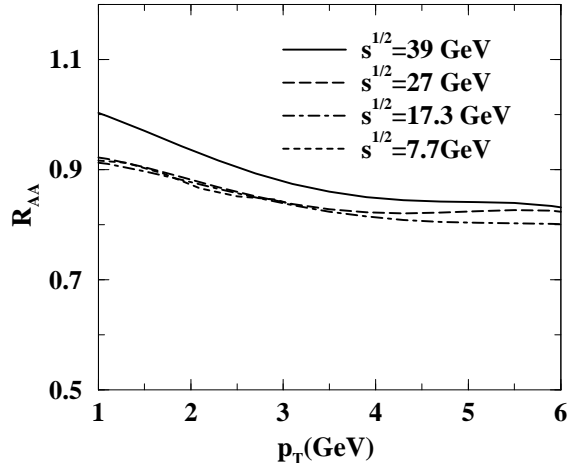


Figure 18: Nuclear suppression factor, R_{AA} as function of p_T for various $\sqrt{s_{NN}}$.

ion collision. If we consider a thermalized ellipsoidal spatial domain of QGP, originated due to non-central nucleus nucleus collisions, with major and minor axes of lengths l_y and l_x (determined by the collision geometry) respectively then the pressure gradient is larger along the minor axis compared to that along the major axis because $l_y > l_x$. Now, pressure gradient is force and hence force along the minor axis is larger than that along the major axis. Consequently, the HQ moves faster in this direction. Therefore, the momentum distribution of electrons originating from the decays of charmed hadrons (D mesons) produced from the charm quark fragmentation will be anisotropic; and since v_2 is the second Fourier's coefficient of the momentum distribution, the spatial anisotropy is thus reflected in the momentum space anisotropy.

v_2 is sensitive to the initial conditions and the equation of state (EoS) of the evolving matter formed in heavy ion collision [86, 87, 88]. Several theoretical attempts has been made in this direction to study both the nuclear suppression factor and elliptic flow of the heavy flavour within a single framework. Although several authors have reproduced the large suppression of high momentum heavy quarks reasonably well yet it is still difficult to explain HQ elliptic flow simultaneously within the same set of initial parameters. It is also imperative to mention that no calculation with radiative energy loss is still able to reproduce heavy flavour elliptic flow. After this brief discussion, we refer the interested readers to Refs. [17, 26, 31, 32, 53, 89, 90, 91, 92] for more interesting aspects of elliptic flow.

10 Summary and Discussions:

In summary, we have tried to give a systematic account of evaluating collisional and radiative transport coefficients of heavy quarks passing through quark gluon plasma. The nuclear suppression factor (R_{AA}) of heavy quarks has been evaluated using Fokker-Planck equation. The present article confines the discussions within perturbative QCD. Recently, ref. [93] finds out the drag force and R_{AA} of charm quarks propagating through thermal-

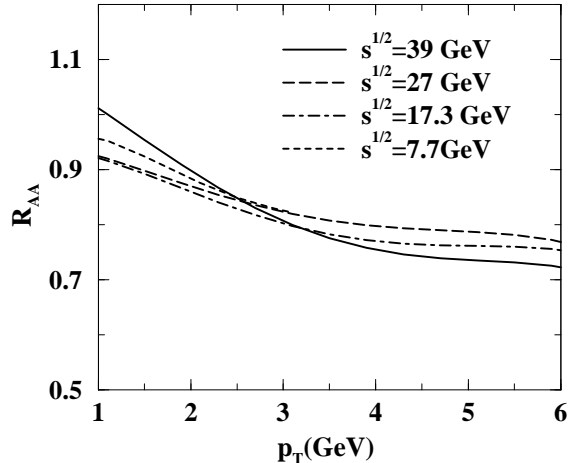


Figure 19: Same as Fig. 18 with enhancement of cross section by a factor of 2.

ized QGP within the framework of both AdS/CFT and AdS/non-CFT. Interested readers are referred to [94, 95] for similar discussions.

We have studied the momentum dependence of transport coefficients and observe that the momentum dependence is crucial in reproducing the trend in the p_T dependence of the experimental data. Also, the dead-cone factor (F_{DC}) weighted by the Gunion-Bertsch spectrum for radiated gluon from heavy quarks is implemented. It is worth mentioning that though the present article speaks at length about elastic as well as bremsstrahlung energy loss of HQs and tells about dominance of the latter in high p_T region; yet there are a plethora of articles which show the importance of elastic energy loss in context of experimental observables in entire momentum range attainable by HQs ([17, 89, 96]). This issue, as a matter of fact, still awaits an unambiguous settlement.

Momentum independent transport coefficients in non-zero baryonic chemical potential region has also been studied and theoretical estimates of the suppression factor is provided. In the Appendix, we have discussed the calculation of elastic transport coefficients within the ambit of QCD hard thermal loop perturbation theory. Also, radiative suppression due to off-shellness of produced partons, which we may call the ‘dead cone due to virtuality’, has also been discussed. This effect of off-shellness of heavy quarks as well as HTL calculations may be extended to encompass radiative processes which, as we have already discussed, will play the most significant part in high energy regime. The calculations of R_{AA} including the aspects just mentioned may be contrasted with the experimental data.

Though [17, 22, 23, 24, 26, 33, 53, 89, 91] attempt to study R_{AA} and v_2 of the heavy quark, yet the role of hadronic matter has been ignored. However, to make the characterization of QGP reliable, the role of the hadronic phase should be taken into consideration and its contribution must be subtracted out from the observables. Although a large amount of work has been done on the diffusion of heavy quarks in QGP, the diffusion of heavy mesons in hadronic matter has received much less attention so far. Recently the diffusion coefficient of D meson has been evaluated using heavy meson chiral perturbation theory [97] and also by using the empirical elastic scattering amplitudes [98] of D

mesons with thermal hadrons. The interactions of D meson with pions, nucleons, kaons and eta particles have been evaluated using Born amplitudes [99] and unitarized chiral effective $D\pi$ interactions [100]. D and B-meson scattering lengths have also been used as dynamical input to study the drag and diffusion coefficients [101, 102]. All these studies observed that the magnitude of both the transport coefficients are significant, indicating substantial amount of interaction of the heavy mesons with the thermal bath. The results may have significant impact on the experimental observables like the suppression of single electron spectra [103] originating from the decays of heavy mesons produced in nuclear collisions at RHIC and LHC energies.

Appendix

Hard Thermal Loop (HTL) approximations and transport coefficients:

We have used $T = 0$ pQCD matrix elements for calculating collisional transport coefficients so far. The t channel divergence due to soft intermediary gluon exchange has been shielded by an ad hoc replacement of t by $t - m_D^2$, where m_D is the (static) Debye screening mass of gluon. Here we use thermal resummed (HTL) gluon propagators [62, 63, 104] for calculating the matrix elements for the processes like $Qq \rightarrow Qq$ and $Qg \rightarrow Qg$, where $Q(q)$ stands for heavy(light) quark and g stands for gluon, for a self-consistent shielding of t channel divergence. Since the light quarks and gluons of thermal bath are hard, *i.e.* their momenta are $\sim T$, we may neglect the vertex correction (assuming $g \ll 1$) arising due to ggg or qqg vertex. The effect of full gluon spectral function on the collisional drag coefficient will be investigated for HQs.

HTL gluon propagator:

For finding out the HTL gluon propagator ($\Delta^{\mu\nu}$) we need HTL approximated self-energy of gluon which goes as an input to $\Delta^{\mu\nu}$ to be used as effective thermal propagator regularizing the t channel divergence. The gluon self-energy in HTL approximation is discussed in detail in Ref. [62, 63]. In this section we give only an outline of the scheme. There are four diagrams which contribute to gluon self-energy (Fig. 20). The loop integrations can be written down easily if we keep in mind that the loop-momentum, $K = (k_0, \vec{k})$ is much larger compared to external gluon momentum, *i.e.* $K \gg P$ which enables us to use simplified ggg vertex [62]. Our goal will be to find out T^2 contributions of self-energy which is the leading behaviour of self-energy in terms of temperature, T . This T^2 contribution of self-energy is called the ‘hard thermal loop’ contribution. We may argue that the hard thermal loop contribution of the gluon self energy is due to momenta $\sim T$ if we look at the generic integral of the type

$$\int_0^\infty k f(k) dk = \frac{\pi^2 T^2}{12}, \quad (47)$$

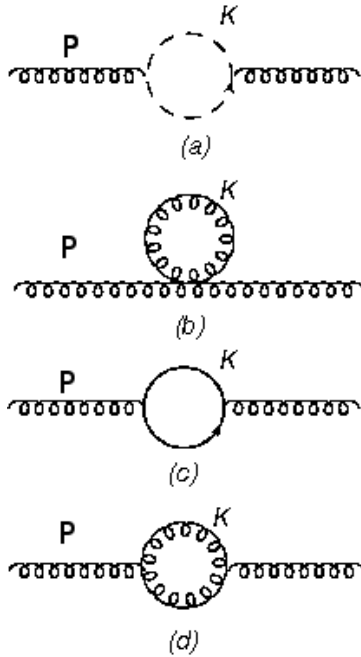


Figure 20: Feynman diagrams contributing to gluon self-energy up to one loop. (a)ghost-gluon loop. (b)four-gluon vertex. (c) quark-antiquark pair creation. (d)three-gluon vertex.

which appears during self-energy calculation. f in Eq. 47 is the distribution function and the leading contribution in Eq. 47 is given by $k \sim T$. Henceforth, we obtain a scale of momentum $\sim T$, which will be called ‘hard’ compared to another ‘soft’ scale $\sim gT$, where $g(\ll 1)$ is the colour charge. HTL gluon propagators are to be used for processes exchanging very soft gluons. As the t channel divergence is equivalent to dominance of soft gluon exchange processes, the use of HTL propagator is justified and consistent.

Now, let us we define the following useful quantities [62] required to write down the gluon propagator in thermal medium. Let u_μ be the fluid four-velocity, with normalization condition $u^\mu u_\mu = 1$. The fluid four-velocity gives rise to two directions; and so any four-vector P^μ can be decomposed into components parallel and perpendicular to the fluid velocity:

$$\begin{aligned}\omega &= P \cdot u \\ \tilde{P}_\mu &= P_\mu - u_\mu(P \cdot u)\end{aligned}\tag{48}$$

where

$$\begin{aligned}P^2 &= \omega^2 - p^2 \\ \tilde{P}^2 &= -p^2\end{aligned}\tag{49}$$

Eqs. 48 and 49 are valid in the local rest frame of fluid, i.e. in a frame where $u = (1, \vec{0})$.

Similarly a tensor orthogonal to u_μ can be defined as,

$$\tilde{g}_{\mu\nu} = g_{\mu\nu} - u_\mu u_\nu \quad (50)$$

The longitudinal and transverse projection tensors, $\mathcal{P}_L^{\mu\nu}$ and $\mathcal{P}_T^{\mu\nu}$ respectively, are defined as [104]

$$\mathcal{P}_L^{\mu\nu} = -\frac{1}{P^2 p^2} (\omega P^\mu - P^2 u^\mu) (\omega P^\nu - P^2 u^\nu) \quad (51)$$

$$\mathcal{P}_T^{\mu\nu} = \tilde{g}_{\mu\nu} + \frac{\tilde{P}_\mu \tilde{P}_\nu}{p^2} \quad (52)$$

which are orthogonal to P^μ as well as to each other, *i.e.*

$$P_\mu \mathcal{P}_L^{\mu\nu} = P_\mu \mathcal{P}_T^{\mu\nu} = \mathcal{P}_{L\nu}^\mu \mathcal{P}_T^{\nu\rho} = 0 \quad (53)$$

But,

$$\mathcal{P}_i^{\mu\rho} \mathcal{P}_{i\nu\rho} = \mathcal{P}_{i\nu}^\mu, \quad i = L, T \quad (54)$$

The HTL gluon propagator, which is given by:

$$\Delta^{\mu\nu} = \frac{\mathcal{P}_T^{\mu\nu}}{-P^2 + \Pi_T} + \frac{\mathcal{P}_L^{\mu\nu}}{-P^2 + \Pi_L} + (\alpha - 1) \frac{P^\mu P^\nu}{P^2} \quad (55)$$

will need HTL approximated longitudinal and transverse self-energies Π_L and Π_T respectively, too. Π_L and Π_T are given by

$$\Pi_L(P) = (1 - x^2) \pi_L(x), \quad \Pi_T(P) = \pi_T(x) \quad (56)$$

where $x = \omega/|\vec{p}|$ ($P \equiv (\omega, \vec{p})$, see Fig. 20) and scaled self-energies π_T and π_L are given by [62],

$$\pi_T(x) = m_D^2 \left[\frac{x^2}{2} + \frac{x}{4} (1 - x^2) \ln \left(\frac{1+x}{1-x} \right) - i \frac{\pi}{4} x (1 - x^2) \right] \quad (57)$$

$$\pi_L(x) = m_D^2 \left[1 - \frac{x}{2} \ln \left(\frac{1+x}{1-x} \right) + i \frac{\pi}{2} x \right] \quad (58)$$

where m_D is the thermal mass of gluon; and is given by $m_D^2 = g^2 T^2 (C_A + N_f/2)/6$, where $C_A = 3$ is the Casimir of adjoint representation of SU(3) and $N_f = 2$ is the number of flavours.

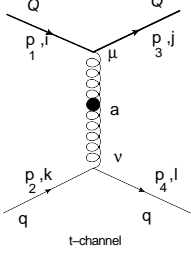


Figure 21: $Qq \rightarrow Qq$ Feynman diagram. Bold lines are for heavy quarks(Q).

Finding out matrix elements for Qq scattering:

From Fig. 21 we can calculate the t-channel matrix element for the process $Qq \rightarrow Qq$. We will use the HTL gluon propagator [62]. Pictorially, an HTL propagator will be denoted by a solid circle. We can write the amplitude in Feynman Gauge ($\alpha = 1$) from Fig. 21 as,

$$-iM_t = \bar{u}(p_3)(-ig\gamma^\mu t_{ji}^a)u(p_1) [-i\Delta_{\mu\nu}] \bar{u}(p_4)(-ig\gamma^\nu t_{lk}^a)u(p_2) \quad (59)$$

where g is strong coupling and $g^2 = 4\pi\alpha_s$. i, j, k, l ($i \neq j, k \neq l$) are quark colours and ‘a’ is the colour of intermediary gluon with polarizations μ, ν . After squaring and averaging over spin and colour as well as using eq. 55 we get,

$$\begin{aligned} \frac{|M_{Qq}|^2}{4C_{Qq}g^4} &= 2\frac{p_4 \cdot \mathcal{P}_T \cdot p_3 p_2 \cdot \mathcal{P}_T \cdot p_1}{(t - \Pi_T)^2} + 2\frac{p_4 \cdot \mathcal{P}_L \cdot p_3 p_2 \cdot \mathcal{P}_L \cdot p_1}{(t - \Pi_L)^2} + 2\frac{p_4 \cdot \mathcal{P}_T \cdot p_1 p_2 \cdot \mathcal{P}_T \cdot p_3}{(t - \Pi_T)^2} \\ &+ 2\frac{p_4 \cdot \mathcal{P}_L \cdot p_1 p_2 \cdot \mathcal{P}_L \cdot p_3}{(t - \Pi_L)^2} + 2A\frac{p_4 \cdot \mathcal{P}_L \cdot p_3 p_2 \cdot \mathcal{P}_T \cdot p_1 + p_4 \cdot \mathcal{P}_T \cdot p_3 p_2 \cdot \mathcal{P}_L \cdot p_1}{(t - \Pi_T)^2 (t - \Pi_L)^2} \\ &+ 2A\frac{p_4 \cdot \mathcal{P}_L \cdot p_1 p_2 \cdot \mathcal{P}_T \cdot p_3 + p_4 \cdot \mathcal{P}_T \cdot p_1 p_2 \cdot \mathcal{P}_L \cdot p_3}{(t - \Pi_T)^2 (t - \Pi_L)^2} \\ &- 2p_4 \cdot p_2 \left[\frac{p_3 \cdot \mathcal{P}_T \cdot p_1}{(t - \Pi_T)^2} + \frac{p_3 \cdot \mathcal{P}_L \cdot p_1}{(t - \Pi_L)^2} \right] \\ &- 2p_3 \cdot p_1 \left[\frac{p_4 \cdot \mathcal{P}_T \cdot p_2}{(t - \Pi_T)^2} + \frac{p_4 \cdot \mathcal{P}_L \cdot p_2}{(t - \Pi_L)^2} \right] \\ &+ p_3 \cdot p_1 p_4 \cdot p_2 \left[\frac{2}{(t - \Pi_T)^2} + \frac{1}{(t - \Pi_L)^2} \right] \\ &+ m^2 \left[2\frac{p_4 \cdot \mathcal{P}_T \cdot p_2}{(t - \Pi_T)^2} + 2\frac{p_4 \cdot \mathcal{P}_L \cdot p_2}{(t - \Pi_L)^2} \right] \\ &- m^2 \left[2\frac{p_4 \cdot p_2}{(t - \Pi_T)^2} + \frac{p_4 \cdot p_2}{(t - \Pi_L)^2} \right] \end{aligned} \quad (60)$$

where $C_{Qq} = \frac{2}{9}$ is the Color factor, $Q^2 \equiv t = (p_1 - p_3)^2$, $A = t^2 - t(\text{Re}\Pi_T + \text{Re}\Pi_L) + \text{Re}\Pi_T \Pi_L^*$ and we have used the following relations,

$$p_1 \cdot \mathcal{P}_L \cdot p_2 = p_3 \cdot \mathcal{P}_L \cdot p_4 = p_4 \cdot \mathcal{P}_L \cdot p_1 = p_2 \cdot \mathcal{P}_L \cdot p_3 \quad (61)$$

as well as,

$$\begin{aligned} \Delta^{\mu\rho} \Delta_{\rho}^{*\nu} &= \frac{\mathcal{P}_T^{\mu\nu}}{(t - \Pi_T)^2} + \frac{\mathcal{P}_L^{\mu\nu}}{(t - \Pi_L)^2} \\ |\Delta|^2 &= \Delta^{\mu\nu} \Delta_{\nu\mu}^* = \frac{2}{(t - \Pi_T)^2} + \frac{1}{(t - \Pi_L)^2} \end{aligned} \quad (62)$$

which can be proven using Eqs. 51, 52, 55 in the rest frame of fluid element.

The $Qg \rightarrow Qg$ scattering contains s , t and u channel diagrams and they can easily be written just like Qq case. There are $|M_t|^2$, $|M_s|^2$ and $|M_u|^2$ as well as the interference of s , t , u channels as opposed to [46] where only s and u channel interference term exists (besides $|M_t|^2$) because gluon momenta are assumed to be much larger than that of HQ.

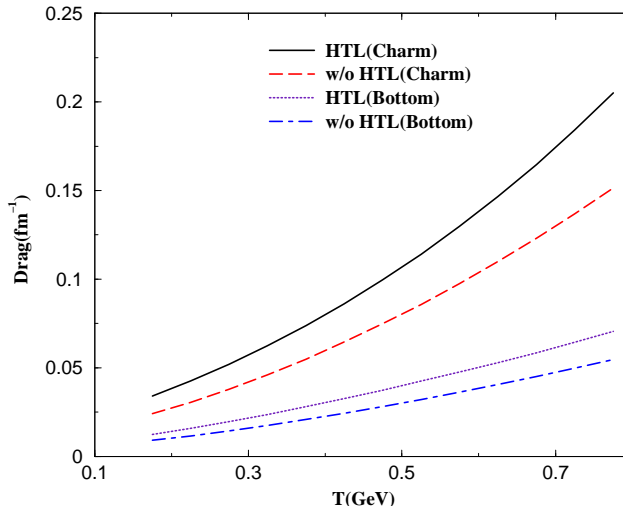


Figure 22: (Color online) Variation of drag of heavy quarks of momentum 1 GeV with temperature.

Results and discussions on Collisional Drag and Diffusion coefficients using HTL propagator:

We have found out the matrix elements for relativistic heavy quark scattering elastically with light quarks and gluons of QGP with arbitrary scattering angle. The variations of drags with temperature for HQs with momentum, $p = 1$ GeV as a function of temperature are displayed in Fig. 22. The results clearly indicate an enhancement and rapid variation of drag using HTL propagator (γ_{HTL}) compared to that in $T = 0$ pQCD (γ). The increase

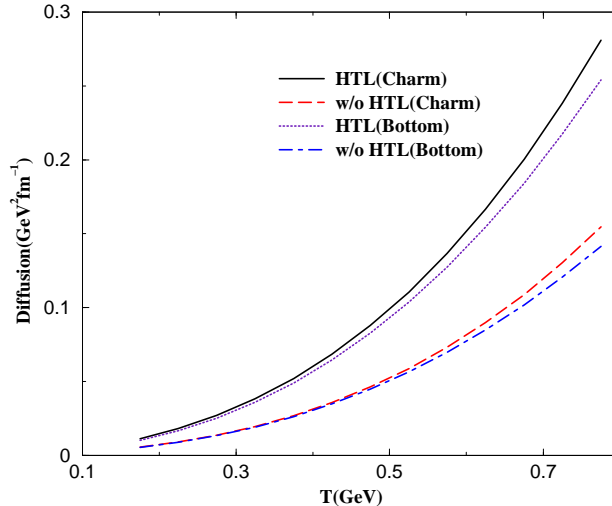


Figure 23: (Color online) Variation of diffusion of heavy quarks of momentum 1 GeV with temperature.

is more prominent for charm than bottom. We have explicitly checked that in the static limit the drag and diffusion using HTL propagator approaches that in $T = 0$ pQCD. γ_{HTL} is greater than γ for the entire momentum range considered here. Again, drag being the measure of energy loss, increase in drag results in more suppression of heavy flavours measured at RHIC and LHC energies. From Fig. 22 we observe that at 400 MeV temperature γ_{HTL} for charm quark is $\sim 33\%$ more than the γ . Whereas, the corresponding difference is $\sim 25\%$ for bottom quarks. We also observe that this difference increases with the increase in temperature. Diffusion coefficients, plotted in fig. 23, seem to be more sensitive to the use of effective propagator in a sense that we observe 100% change between the diffusion using HTL propagator (D_{HTL}) and that in $T = 0$ pQCD (D) at $T = 400$ MeV and this difference increases with T . Though unlike drag, this difference is not much (3.5%) for a difference in charm and bottom quark masses.

[46] also calculates the energy loss of heavy quarks using HTL propagator and gets a drag which is 16% less than that obtained in the present paper at HQ momentum 4 GeV and $T = 250$ MeV. [17] calculates diffusion coefficient of a non-relativistic heavy quark in leading order as well as in next to leading order. The leading order result surpasses the present result by 25% at $T = 300$ MeV and at a very low momentum (0.2 GeV) of HQ.

However, radiative transport coefficients like drag are also needed for we have seen that radiation becomes very important in high energy regime. We can even extend the present calculation of collisional drag and diffusion using HTL propagator to radiative domains; but that will increase the complexity of problem.

Recent efforts of generalizing GB formula:

Gunion-Bertsch formula is derived in the mid-rapidity region and there is another very recent development in this field proposed in [105] where a generalized Gunion-Bertsch formula for arbitrary forward and backward rapidity region has been derived. This modification will be needed when one needs to compute cross sections and rates. Now, this calculation involves two parts (a) keeping a factor $(1-x)^2$, where x is the fraction of light cone momentum carried by the emitted gluon and (b) combination of calculations obtained from both $A^+ = 0$ and $A^- = 0$ gauge conditions for emitted gluon polarization. The final form of $M_{qq' \rightarrow qq'g}$ can be written as follows:

$$|M_{qq' \rightarrow qq'g}|^2 = 12g^2 |M_{qq' \rightarrow qq'}|_{sa}^2 (1 - \bar{x})^2 \times \frac{q_\perp^2}{k_\perp^2 (\vec{q}_\perp - \vec{k}_\perp)^2}, \quad (63)$$

where

$$\bar{x} = \frac{k_\perp e^{|\eta|}}{\sqrt{s}}, \quad (64)$$

where η is the rapidity of the emitted gluon. With this, the exact differential cross-section $(\frac{d\sigma}{d\eta})$ for the process $qq' \rightarrow qq'g$ is shown to be reproduced by using Eq. 63 for all rapidity ranges.

In all these calculations, we tacitly assume that the incoming jet is hard enough so that eikonal approximation (straight path) for it is always valid. But there has been a recent attempt of relaxing the eikonal approximation in [106] and 15-20% suppression in the differential cross-section of $2 \rightarrow 3$ processes for moderately hard jets because of the noneikonal effects has been found.

Dead cone effect revisited and other aspects of energy loss

[107] computes the HQ-LQ \rightarrow HQ-LQ-g scattering amplitude for soft gluon emission and finds out a general expression for radiative suppression factor for dead cone effect. In the limit $m \ll \sqrt{s}$ and $\theta \rightarrow 0$, they reproduce Eq.31. In the backward rapidity region the gluon emission does not depend on the mass and in $\theta \sim \pm\pi$ region there is no suppression, in contrast with what we get from [68](see [70] also). [108] evaluates the HQ energy loss employing the generalized dead-cone factor in [107]. They report similar energy loss for both massless and massive quark jets.

However, the high energy quarks and gluons produced from the hard collisions of the partons from the colliding nucleons are off-shell and their colour fields are stripped off, *i.e.* they have no field to radiate. Therefore, the partons' virtuality creates its own dead-cone which may be large depending on the magnitude of the virtuality. The forbidden zone around the direction of motion of the partons due to its virtuality will here be called virtual dead cone. If the virtuality does not disappear before the hadronization of the QGP then the dead cone suppression due to virtuality will play a decisive role in QGP diagnostics by jet quenching. The conventional dead cone (due to the mass of the quark) becomes important when the virtuality of the quarks reduces to zero.

For the demonstration of suppression of soft gluon radiation due to virtuality, we can take up the $e^+e^- \rightarrow Q\bar{Q}g$ process, where Q is heavy quark. The spectrum of the soft gluons emitted by the virtual quarks can be shown to be [109]

$$F = 4\beta^2 \left(\frac{\frac{V^4}{k_0^2 E^2} + \frac{4V^2}{k_0 E} + 4\sin^2\theta}{\left(\frac{V^4}{k_0^2 E^2} + \frac{4V^2}{k_0 E} + 4(1 - \beta^2 \cos^2\theta)\right)^2} \right), \quad (65)$$

where external quarks are assumed to be on the verge of being on-shell so that Dirac's equation can be applied. V is the virtuality parameter defined by the equation, $V^2 = q^2 - m^2$ where q^2 is four-momentum square of external virtual particles; and m is its mass, if any. $q^2 = m^2$ implies $V = 0$, i.e. the particle becomes on-shell. One can show that the spectrum is that of gluons emitted from on-shell quarks when $V = 0$. k_0 is the energy of the soft gluon emitted at angle θ with the parent quark whose velocity is β and energy is E . The virtuality is replaced by $V = \sqrt{q^2 - m^2} = \sqrt{E^2 - p^2 - m^2}$. The emitted gluon carry a fraction of parent parton energy consistent with $|\vec{p}_i| \sin\theta \gg k_0$ (for dominance of soft gluon emission). Different limits of F given in Eq. 65 will be worth exploring.

(i) For zero virtuality ($V = 0$) of the massive quark, Eq. 65 reduces to the conventional dead cone factor (Fig. 24):

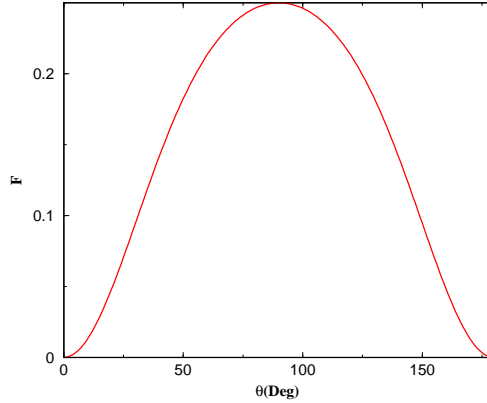


Figure 24: Plot of the spectrum F in $V = 0$ limit (Eq. 66), $m = 1.5$ GeV, $\beta = 0.5$

$$F \longrightarrow \frac{\beta^2 \sin^2\theta}{(1 - \beta^2 \cos^2\theta)^2} \quad (66)$$

This is the well-known conventional dead cone for a gluon emitted by a massive quark for large angles. The divergence of the factor is shielded by the quark mass or virtuality through $\beta (< 1)$. In fact, for on-shell quarks with small θ one can show that Eq. 66 (see [68]) boils down to:

$$F = \frac{1}{\theta^2} \frac{1}{(1 + \theta_0^2/\theta^2)^2}, \quad \theta_0 = m/E \quad (67)$$

and for highly virtual quarks (large V) the F can be written as:

$$F = \frac{\omega^2}{E^2} \quad (68)$$

(ii) Now, the light quark limit ($\beta = 1$) can be investigated. For $V = 0$, $\beta = 1$,

$$F \sim \frac{1}{\sin^2\theta} \quad (69)$$

For light quarks Eq. 69 ensures the absence of dead-cone suppression at $\theta = 0$ and π for vanishing virtuality.

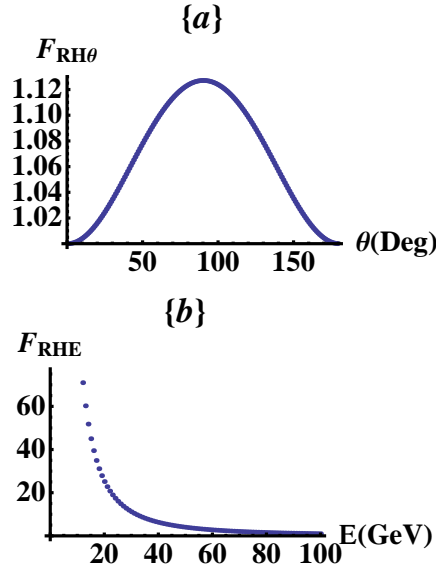


Figure 25: (Colour online) The variation of (a) $F_{RH\theta}(E, \theta)$, defined in the text with θ for $E = 1.5$ GeV, (b) with E for $\theta = \pi/4$ for virtual heavy quarks. The results displayed in this figure are evaluated for heavy quark mass, $m = 1.27$ GeV, emitted gluon energy, $k_0 = 20$ MeV and $\beta = 0.5$. The quark virtuality is defined as $V^2 = E^2 - \beta^2 E^2 - m^2$.

In Fig. 25 the suppression of the energy loss, F for heavy quarks is displayed. The variation of $F_{RH\theta} = F(E = 1.5\text{GeV}, \theta)/F(E = 1.5\text{GeV}, \theta = 0)$ with θ is depicted in Fig. 26(a). It is interesting to note that for vanishingly small virtuality the suppression is similar to that of a conventional dead cone that appear for massive on-shell quarks (Fig 24). In Fig. 25 (b) the variation of $F_{RHE} = F(E, \theta = \pi/4)/F(E = 100\text{GeV}, \theta = \pi/4)$ with E is displayed for heavy quarks. For large virtuality (which increases with parton energy, E) the suppression is large.

Fig. 26 illustrates the suppression of the energy loss for light quarks. In Fig. 26 (a) the variation of $F_{RL\theta} = F(E = 3\text{GeV}, \theta)/F(E = 3\text{GeV}, \theta = 0)$ with θ is shown for light partons. It is important to note that the variation of $F_{RL\theta}$ with θ for light quark with low virtuality is drastically different from the corresponding quantity, $F_{RH\theta}$ for heavy quark. This is obvious because for low virtuality the light partons are not subjected to any dead

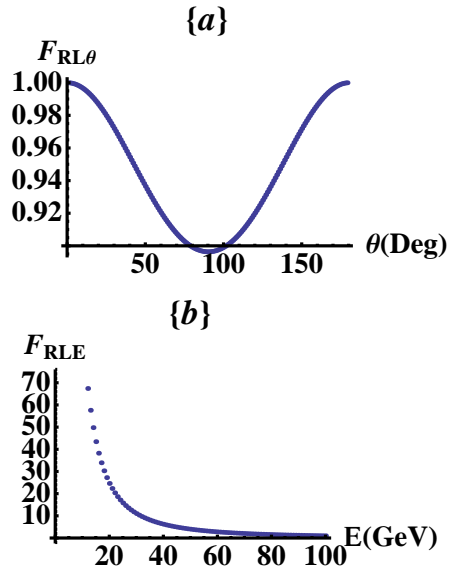


Figure 26: (Colour online) The variation of (a) $F_{RL\theta}(E, \theta)$, defined in the text with θ for $E = 3$ GeV, (b) with E for $\theta = \pi/4$ for virtual light partons. The results displayed in this figure are evaluated for vanishing quark mass, $\beta = 0.95$ and emitted gluon energy, $k_0 = 10$ MeV. The quark virtuality is defined as $V^2 = E^2(1 - \beta^2)$.

cone suppression at $\theta = 0$ and π unlike heavy quarks. Moreover, the $\sin^{-2}\theta$ behaviour for light quarks (Eq. 69) ensures a minimum at $\theta = \pi/2$ as opposed to a maximum at the same θ for heavy quarks. In Fig. 26 (b) the variation of $F_{RLE} = F(E, \theta = \pi/4)/F(E = 100\text{GeV}, \theta = \pi/4)$ with E is depicted. We note that the suppression is large for high E and the behaviour of F_{RLE} is similar to F_{RHE} which indicates that the suppression due to virtuality overwhelm the effects due to the conventional dead cone.

The energy loss ($\Delta E(L)$) of quarks as a function of path length (L) traversed by the off-shell parton in vacuum can be evaluated (see [110] for details) by using the emitted gluon spectrum given by Eq. 65. The results are displayed in Fig. 27. We note that the energy loss of light and heavy quarks differ significantly at large path length or time when the propagating quarks acquire enough field to radiate. However, at small path length the value of ΔE for light and heavy quarks are similar.

When we want to talk about radiative energy loss of high energy partons we mean the absorption of radiation given off is absorbed in the medium. So, we must take into account the interaction of emitted radiation with the medium. Consequently, the dispersion relation of the emitted gluon should change. This change in gluon dispersion relation is encoded in the thermal quark self energy; and as the inverse of imaginary part of self energy gives radiation production rate, the formation time of radiation is also modified. This effect of modified dispersion relation of emitted gluon (or photon) is called Ter-Mikaelian (TM) effect [65]. The QCD analogue of TM effect is discussed in [111, 112]. [53] implements TM effect by replacing $x^2 m^2$ by $x^2 m^2 + (1 - x)m_D^2$, where m_D is thermal mass of gluon. However, [111] repeats the single, double and multiple scattering calculations of [48] by assuming a modified dispersion relation, $k^2 = \omega_0^2(T)$, of emitted

gluon. ω_0 parametrizes gluon self energy in medium. [111] shows that in the phase space region where abelian radiation does not occur, the gluon radiation is suppressed due to polarization properties of the medium. [112, 113] extends the results of [111] using 1-Loop HTL self-energy of gluons. [113] shows a $\sim 30\%$ decrease in 1st order in opacity fractional energy loss for heavy quarks of 10 GeV energy when TM effect is taken into account. Whereas, [53] shows ~ 1.5 times increase in radiative energy spectra per unit length when gluon thermal mass is taken into consideration. Such changes indicate that one can barely neglect the effect of gluon interaction with medium while probing QGP.

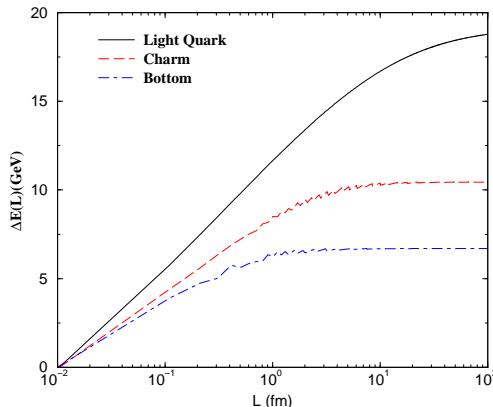


Figure 27: Variation of energy loss, ΔE as a function of path traversed, L in vacuum. The energy of the quark is taken as $E = 20$ GeV.

So far, we have talked about the energy loss of HQs in an infinite medium. But, how does the energy loss depend on the size of medium? [50] shows that length dependent energy loss $\Delta E(L) \propto L^2$, when we are considering the coherent region, *i.e.* the emitted gluon energy is soft and is within the factorization and the Bethe-Heitler limits (see [114]). When gluon energy (k_0) is of the order of that of parent parton (E), the energy loss per unit length becomes independent of length of medium. This is the limit ($k_0 \sim E$) when evaluation of transport coefficients without addressing to size of medium works more efficiently.

There is also a path integral approach of radiative energy loss proposed in [115]. Path integral approach is shown to be equivalent to the approach of [50] in [114]. An alternate formalism (GLV) proposed in [51, 116] performs a systematic expansion in opacity (the mean number of jet scatterings). Opacity is quantitatively given by $\bar{n} = L/\lambda$, where L is the target thickness and λ is the mean free path. One analytic limit applies to plasmas where mean number of scattering is small [49]. The other limit applies to thick plasma where $\bar{n} \gg 1$ [50].

Acknowledgements:

SM and TB are supported by DAE, Govt. of India. SKD acknowledges the support by the ERC StG under the QGPDyn Grant n. 259684. The authors thank Jan-e Alam and

Md. Younus for fruitful discussions and critical reading of the manuscript. The authors also take the opportunity to thank the anonymous reviewers for their relevant suggestions which have undoubtedly helped to increase the quality of manuscript.

References

- [1] D. J. Gross and F. Wilczek, Phys. Rev. Lett **30**, 1343 (1973).
- [2] D. J. Gross and Frank Wilczek, Phys. Rev. D **8** , 3633 (1973).
- [3] H. D. Politzer, Phys. Rev. Lett **30**, 1346 (1973).
- [4] J. C. Collins and M. J. Perry, Phys. Rev. Lett **34**, 1353 (1975).
- [5] N. Cabibbo and G. Parisi, Phys. Lett. B **59**, 67 (1975).
- [6] F. Karsch, Lect. Notes Phys. **583** 209(2002), arXiv:hep-lat/0106019; Nucl. Phys. A **698**, 199(2002).
- [7] S. Borsányi *et al.* , JHEP **11**, 077(2010).
- [8] Y. Aoki, G. Endrődi, Z. Fodor, S. D. Katz, and K. K. Szabó, Nature **443**, 675(2006).
- [9] S. Borsnàyi *et al.* , J. Phys. G: Nucl. Part. Phys. , **38**, 124101(2011).
- [10] P. Kovtun, D. T. Son and O. A. Starinets, Phys. Rev. Lett. **94**, 111601 (2005).
- [11] A. Adams, L. D. Carr, T. Schaefer, P. Steinberg, J. E. Thomas, New J. Phys. **14**, 115009(2012). arXiv:1205.5180 [hep-th].
- [12] S. S. Adler *et al.* (PHENIX Collaboration), Phys. Rev. Lett. **96**, 032301 (2006).
- [13] B. I. Abeleb *et al.* (STAR Collaboration), Phys. Rev. Lett. **98**, 192301 (2007).
- [14] B. Abelev *et al.*, (ALICE collaboration), arXiv:1205.6443v1 [hep-ex].
- [15] A. Adare *et al.* (PHENIX Collaboration), Phys. Rev. Lett. **98**, 172301 (2007).
- [16] A. Rossi (for ALICE collaboration), Quark Matter, 2011, May 23-28, Annecy, France. e-print-arXiv:1106.5931 [hep-ex].
- [17] G. D Moore and D. Teaney, Phys. Rev. C **71**, 064904(2005).
- [18] C. M. Ko and W. Liu, Nucl. Phys. A **783**, 23c(2007).
- [19] A. Adil and I. Vitev, Phys. Lett. B **649**, 139(2007).
- [20] N. Armesto, M. Cacciari, A. Dainese, C.A. Salgado and U.A. Wiedemann, Phys. Lett. B **637** 362(2006).
- [21] P. B. Gossiaux and J. Aichelin, Phys. Rev. C **78**, 014904 (2008).

- [22] S. K. Das, J. Alam and P. Mohanty, Phys. Rev. C **80**, 054916(2009).
- [23] S. K. Das, J. Alam and P. Mohanty, Phys. Rev. C **82**, 014908(2010).
- [24] S. K. Das, J. Alam, P. Mohanty and B. Sinha, Phys. Rev. C **81**, 044912(2010).
- [25] J. Uphoff, O. Fochler, Z. Xu and C. Greiner, Phys. Rev. C **84** 024908(2011).
- [26] W. M. Alberico *et al.*, Eur. Phys. J. C **71** 1666(2011).
- [27] S. Mazumder, T. Bhattacharyya, J. Alam and S. K. Das, Phys. Rev. C **84**, 044901(2011).
- [28] M. Younus and D. K.Srivastava, J. Phys. G: Nucl. Part. Phys. **39**, 095003(2012).
- [29] M. G. Mustafa, D. Pal, D. K. Srivastava and M. H. Thoma. Phys. Lett. B, **428**, 234(1998).
- [30] C. Young, B Schenke, S. Jeon and C. Gale, Phys. Rev. C **86**, 034905(2012).
- [31] S. Cao, G. Qin and S. Bass, arXiv:1205.2396 [nucl-th].
- [32] T. Lang, H. Hees, J. Steinheimer and M. Bleicher, arXiv:1208.1643 [hep-ph].
- [33] S. K. Das, V. Chandra, J. Alam, arXiv:1210.3905 [nucl-ph].
- [34] S. Chakravorty and D. Syam, Lett. Nuovo Cim. **41**, 381(1984).
- [35] J. Alam, B. Sinha and S. Raha, Phys. Rev. Lett. **73**, 1895(1994).
- [36] B. Svetitsky, Phys. Rev. D **37**, 2484(1988).
- [37] H. M. Antia, *Numerical Methods for Scientists and Engineers*, (Tata McGraw-Hill, 1991).
- [38] M. L. Mangano, P. Nason and G. Ridolfi, Nucl. Phys. B **373**, 295(1992).
- [39] H. van Hees, R. Rapp, Phys. Rev. C **71**, 034907(2005).
- [40] B. L. Combridge, Nucl. Phys.B **151**, 429(1979).
- [41] M. G. Mustafa, D. Pal and D. K. Srivastava, Phys. Rev. C **57**, 889(1998).
- [42] H. Van Hees, M. Mannarelli and R. Rapp, Eur. Phys. J. C, **61**, 799(2009).
- [43] P. B. Gossiaux, J. Aichelin and T. Gousset, Prog. of Th. Phys. Suppl., **193**, 110(2012).
- [44] M. He, R. J. Fries and R. Rapp, Phys. Rev. C **86**, 014903(2012).
- [45] W. R. Leo, *Techniques for Nuclear and Particle Physics Experiments*, (Springer-Verlag Berlin Heidelberg, 1987).

- [46] E. Braaten and M. H. Thoma, Phys. Rev. D **44**, 2625(R) (1991).
- [47] M. Gyulassy, M. Plümer, M.H. Thoma, X.N. Wang, Nucl. Phys. A **538** 37c(1992).
- [48] X.N. Wang, M. Gyulassy, M. Plümer, Phys. Rev. D **51**, 3436(1995).
- [49] M. Gyulassy, X.N. Wang, Nucl. Phys. B **420**, 583(1994).
- [50] R. Baier *et al.*, Phys. Lett. B 345 **277**(1995); R. Baier *et al.* , Nucl. Phys. B **483**, 291(1997).
- [51] M. Gyulassy, P. Levai, I. Vitev, Phys. Rev. Lett **85**, 5535(2000).
- [52] L.D. Landau and I.Ya. Pomeranchuk, Dokl. Akad. Nauk SSSR 92 **535**, 735(1953); A.B. Migdal, Phys. Rev. **103**, 1811(1956).
- [53] P.B. Gossiaux, J. Aichelin, T. Gousset and V. Guiho J. Phys.G **37**, 094019(2010).
- [54] Y.S. Kim and M. E. Noz, Am. J. Phys. **50**, 721(1982) ; L. McLerran arXiv:hep-ph/9903536 ; B. Zwiebach, *A first course in string theory*, (Cambridge University Press, New York 2009).
- [55] Energy Loss of Quarks by Gluon Radiation in Deconfined Matter, R. Thomas Ph. D. Thesis, Institut für Theoretische Physik 2003.
- [56] J. F. Gunion and G. Bertsch, Phys. Rev. D **25**, 746(1982).
- [57] S. K. Das and J. Alam, Phys. Rev. D **82**, 051502(R) (2010).
- [58] R. Abir, C. Greiner, M. Martinez, and M. G. Mustafa, Phys. Rev. D **83**, 011501(R) (2011).
- [59] T. Bhattacharyya, S. Mazumder, J. Alam and S. K. Das, Phys. Rev. D **85**, 034033(2012).
- [60] F. A. Berendes *et al.*, Phys. Lett. B **103**, 124(1981).
- [61] S. M. H. Wong, Nucl. Phys. A **607**, 442(1996).
- [62] M. Le Bellac, *Thermal Field Theory*, (Cambridge University Press, Cambridge 1996).
- [63] J. I. Kapusta and C. Gale, *Finite Temperature Field Theory*, (Cambridge Monograph on Mathematical Physics, Cambridge University Press, Cambridge 2006).
- [64] O. Kaczmarek and F. Zantow Phys. Rev. D **71**, 114510(2005).
- [65] S. Klein, Rev. Mod. Phys., **71**, 1501(1999).
- [66] M. H. Thoma, Phys. Rev. D **49**, 451(1994).

- [67] T. S. Biró, E. Van Doorn, B. Müller, M. H. Thoma and X. N. Wang, Phys. Rev. C **48**, 1275 (1993).
- [68] Y. L. Dokshitzer and D. E. Kharzeev, Phys. Lett. B **519**, 199(2001).
- [69] J.D. Jackson, *Classical Electrodynamics* (John Wiley and Sons Pvt. Ltd. , New York 1998).
- [70] From Higgs to Top to Color. K. M. Paul Ph. D. Thesis, University of Illinois at Urbana-Champaign, 2002.
- [71] J. D. Bjorken, Phys. Rev. D **27**, 140 (1983).
- [72] S. Turbide, C. Gale, S. Jeon and G. D. Moore, Phys. Rev. C **72**, 014906(2005).
- [73] C. Peterson *et al.*, Phys. Rev. D **27**, 105(1983).
- [74] R. J. Fries, V. Greco, P. Sorensen, Ann. Rev. Nucl. Part. Sci. **58**, 177(2008),
V. Greco, H. van Hees and R. Rapp, AIP Conf. Proc. **1422**, 117(2012).
- [75] R. C. Hwa and K. Kajantie, Phys. Rev. D **32**, 1109(1985).
- [76] S. Mazumder and J. Alam, Phys. Rev. C **85**, 044918(2012).
- [77] T. Sakaguchi (PHENIX collaboration), PoS CPOD2009 (2009) 055. arXiv:0908.3655 [hep-ex].
- [78] B. I. Abelev (Star Collaboration), arXiv:0909.4131 [nucl-ex].
- [79] J. M. Heuser (CBM collaboration), J. Phys. G **35**, 044049(2008).
- [80] O. Ristea (for the BRAHMS collaboration) Romanian Reports in Physics, **56**, 659(2004).
- [81] A. Andronic, P. Braun-Munzinger and J. Stachel, Nucl. Phys. A **772**, 167(2006).
- [82] D. Kharzeev and M. Nardi, Phys. Lett. B **507**, 121(2001).
- [83] R. J. Glauber, in *lecture in Theoretical Physics*, edited by W. E. Brittin and L. G. Dunham (Interscience, N.Y., 1959), Vol **1**, p. 315.
- [84] B. B. Back *et al.* (PHOBOS Collaboration), Phys. Rev. C **70**, 021902(2004).
- [85] R. D. Field, *Application of Perturbative QCD*, (Addison-Wesley Pub. Company, N.Y. 1989).
- [86] T. Hirano, Naomi van der Kolk and A. Bilandzic, Lect. Notes Phys. **785** 139(2010).
- [87] P. Huovinen and P. V. Ruuskanen, Ann. Rev. Nucl. Part. Sci. **56**, 163(2006).
- [88] D. A. Teaney, arXiv:0905.2433 [nucl-th].

- [89] H. van Hees, V. Greco and R. Rapp, Phys. Rev. C **73**, 034913(2006).
- [90] H. van Hees, M. Mannarelli, V. Greco and R. Rapp, Phys. Rev. Lett. **100**, 192301(2008).
- [91] Y. Akamatsu, T. Hatsuda and T. Hirano, Phys. Rev. C **79**, 054907(2009) .
- [92] S. K. Das and J. Alam, arXiv:1008.2643 [nucl-th], arXiv:1101.3385 [nucl-th].
- [93] S. K. Das and A. Davody, arXiv:1211.2925 [hep-ph]
- [94] S. Gubser, Phys.Rev. D **74**, 126005(2006).
- [95] G.C. Giecold, JHEP **06**, 002(2009).
- [96] M. G. Mustafa, Phys. Rev. C **72**, 014905(2005).
- [97] M. Laine, JHEP **04** 124, 2011, arXiv:1103.0372 [hep-ph].
- [98] M. He, R. J. Fries and R. Rapp, Phys. Lett. B **701**, 445(2002).
- [99] S. Ghosh, S. K. Das, S. Sarkar and J. Alam, Phys. Rev. D **84**, 011503(2011).
- [100] L. Abreu, D. Cabrera, F. J. Llanes-Estrada and J. M. Torres-Rincon, Annals Phys. **326**, 2737 (2011); L. Abreu, D. Cabrera and J. M. Torres-Rincon, arXiv:1211.1331 [hep-ph].
- [101] S. K. Das, S. Ghosh, S. Sarkar and J. Alam, Phys. Rev. D **85**, 074017(2012).
- [102] D. Cabrera, L. M. Abreu, F. J. Llanes-Estrada, J. M. Torres-Rincon, Nucl. Phys. A **00** 1(2013). arXiv:1303.1303 [hep-ph].
- [103] Santosh K. Das, Sabyasachi Ghosh, Sourav Sarkar, Jan-e Alam, Phys. Rev. D **88**, 017501(2013). arXiv:1303.2476 [nucl-th]
- [104] H. Heiselberg and Xin-Nian Wang, Nucl. Phys. B **462**, 389(1996).
- [105] O. Fochler, J. Uphoff, Z. XU and C. Greiner, arXiv:1302.5250 [hep-ph].
- [106] R. Abir, Phys. Rev. D **87**, 034036(2013). arXiv: 1301.1839 [hep-ph].
- [107] R. Abir, C. Greiner, M. Martinez, M. G. Mustafa and J. Uphoff, Phys. Rev. D **85**, 054012(2012).
- [108] R. Abir, U. Jamil, M. G. Mustafa and D. K. Srivastava Phys. Lett. B **715**, 183(2012).
- [109] T. Bhattacharyya and J. Alam, Int. J. of Mod. Phys. A **28**, 1350031(2013), arXiv: 1204.3992[hep-ph].
- [110] B. Z. Kopeliovich, I. K. Potashnikova, I. Schmidt, Phys. Rev. C **82**, 037901(2010).
- [111] B. Kämpfer and O. Pavlenko, Phys. Lett. B **477**, 171(2000).

- [112] M. Djordjevic and M. Gyulassy, Phys. Lett. B **560**, 37(2003).
- [113] M. Djordjevic, Phys. Rev. C **68**, 034914(2003).
- [114] R. Baier, D. Schiff and B.G. Zakharov, Ann. Rev. Nucl. Part. Sci. **50**, 37(2000).
- [115] B. G. Zakharov, JETP Lett. **63**, 952(1996); B. G. Zakharov, *ibid.* **64**, 781(1996);
B. G. Zakharov, *ibid.* **6**, 615(1997).
- [116] M. Gyulassy, P. Levai and I. Vitev, Nuclear Physics B **594**, 371(2001).